공학석사 학위논문

공진 수로 내장형 슬릿 케이슨 방파제의 반사특성

Reflection Characteristics of a Slit Caisson Breakwater with Embedded Resonant Channels

지도교수 이중우, 박우선

2015년 2월

한국해양대학교 해양과학기술전문대학원

해양과학기술융합학과

김정석

A Thesis for the Master Degree of Engineering

Reflection Characteristics of a Slit Caisson Breakwater with Embedded Resonant Channels

Advisors Joong Woo Lee

Woo Sun Park

February, 2015

Korea Maritime and Ocean University

Department of Convergence Study on Ocean Science and Technology

Jeong Seok Kim

본 논문을 김정석의 공학석사 학위논문으로 인준함.

위원장 이 진 학 (인)

위 원 이 중 우 (인)

위 원 박 우 선 (인)

2015년 01월 23일

한국해양대학교 해양과학기술전문대학원

Reflection Characteristics of a Slit Caisson Breakwater with Embedded Resonant Channels

Jeong Seok Kim

Korea Maritime and Ocean University

Department of Convergence Study on Ocean Science and Technology

Abstract

Interaction of waves and a permeable structure is an attractive subject to coastal engineer. In present study, a new concept slit caisson breakwater is proposed, which has embedded channels for fluid resonance in the channel. When the amplified flow is passing through the slit plate, the incident wave energy is dissipated by flow separations. In order to evaluate wave energy dissipation performance of the breakwater, this study has focused on the wave reflection from the breakwater by using numerical simulation and hydraulic model test. The numerical experiment was carried out by Galerkin's finite element model based on the linear potential theory, and the hydraulic model test was performed in a two-dimensional wave flume at KIOST. Comparison of the numerical results with hydraulic model test results shows proper agreement over wide wave periods. The performance of slit caisson breakwater with the embedded resonant channels was tested with various design of the embedded channel. This breakwater has advantages compared with conventional slit wall caisson breakwater. First, the channel design to control the target wave condition is easy and applicable to long wave periods for dissipating wave energy. Second, this breakwater has structural safety of slit members because the members are not exposed to impact load at

near free surface, directly. When the incident wave period and natural period of water column in the channel were matched, the considerable wave energy dissipation was occurred. From this reason, the wave load acting on the breakwater is decreased by wave energy dissipation. The wave reflection characteristics were affected by the porosity of slit plate, the channel width, and the number of channels. Therefore, this breakwater is expected to economical and efficient coastal structures.

Key words: Wave reflection, Energy dissipation, Resonant channel, Slit plate, FEM, Caisson breakwater.

공진 수로 내장형 슬릿 케이슨 방파제의 반사특성

김 정 석

한국해양대학교 해양과학기술전문대학원

해양과학기술융합학과

Abstract

연안 공학자들에게 파랑하중에 대한 유공구조물의 상호작용은 흥미로운 주제이다. 본 연구에서는 새로운 개념의 공진수로를 이용한 슬릿 케이슨 방파제를 제안하고자 한다. 공진 수로 내장형 슬릿 케이슨 방파제는 수로 내의 유체의 공진을 유도하여 증폭된 흐름이 슬릿형 유공판을 통과함으로써 흐름분리현상에 의한 에너지 소산효과로부터 제체 전면의 반사파를 저감시키는 것을 목적으로 한다. 본 방파제의 파랑에너지의 소산성능은 제체 전면의 반사율로 평가하였으며, 수치해석 및 수리실험을 통하여 반사율을 추정하였다. 본 수치해석은 선형포텐셜이론에 기초한 Galerkin의 유한요소모델을 이용하였으며, 한국해양과학기술원(KIOST)의 2차원 조파수조에서 수행한 수리모형실험의 결과와 비교를 통하여 다양한 입사파주기에서의 수치해석결과에 대한 타당성을 입증하였으며, 다양한 공진 수로 내장형 유공방파제 형상이 반사특성에 미치는 영향을 분석하였다. 본 방파제는 종래의 유공벽을 이용한 케이슨 방파제와 비교하여 다음의 장점을 갖는다. 목표 차단파랑 및 장주기 파랑의 제어를 위한 수로의 설계가 용이하며, 유공부가 쇄파력이 집중되는 수면부근에 노출되지 않아 유공부의 부재들의 구조안정성을 갖는다. 입사파의 주기와 수로 내부 유체의 고유주기가 일치할 때에 적절한 파랑에너지 소산효과가 나타났으며, 이는 파랑에너지 소산에 의한 제체에 작용하는 파력이 저감됨을 의미한다. 본 방파제는 경제적이며 효과적인 해안구조물로 적용될 수 있을 것으로 기대된다. 방파제 전면 유동장의 반사특성은 유공판의 유공율, 수로의 폭 그리고 수로의 개수에 의해 지배적인 영향을 받았다.

Table of Contents

List of Tables

List of Figures

CHAPTER 1
INTRODUCTION

1.1 Research Background

In the sea, interaction of wave and structure is shown very complex phenomenon. The numerical analysis of wave breaking condition is hard to predict, also the non-linear characteristics of high wave height and motion of structure in wave condition. So, previous researches were performed using the linear wave theory in fluid domain, and assuming the amplitude of very small structure motion. These researches had been validated to use basis data. For coastal researchers and engineers, the interaction of waves and the permeable structures is an attractive subject. There permeable structures are used to protect coastal area from wave action, such as harbors, inlets and beaches. The permeable structures are proposed to various type in researches also had been applied to coastal area, such as rubble mound breakwater and slit type structure.

Nowadays, various types of breakwaters are being constructed for protect coastal area, from conventional rubble mound breakwater to floating breakwater. One of the recent trends for the breakwater in Korea is to construct slit-type (perforated) breakwater for reducing the reflected waves. It is related with the calmness of harbor area and reducing wave force on breakwaters. Prediction of the reflection and transmission of waves from permeable structures is important to the estimation of the calmness of harbor area and to improve the economics of the breakwater construction.

The slit-type breakwater is considered here consists of a vertical cylinders and a embedded channel. The cylinders induce energy dissipation which is caused by flow separation. This type of energy dissipation mechanism are might effective to reducing wave action in a harbor. A slit-type breakwater has a number of desirable advantages. It can reduce not only wave reflection and wave transmission over the structure but also wave force acting on the breakwater unit. The function of these breakwater is evaluated by calculating the reflection and transmission of waves.

However, slit-type or perforated breakwater has several weakness. First, the slit of the breakwater is exposed to the impact wave loads, directly. The cylinder array are consist of thin columns, Therefore the structural problem comes up. Second, function of conventional slit-type breakwater is effective only for the short waves. The minimum wave reflection on the slit-type breakwater is shown at the $B/(L\cos\theta) \simeq 0.2$ (Kim, 1998). For the proper energy dissipation, it is need that the wide width of breakwater in horizontal direction with respect to incident wave length. But, the chamber width (B) is limited by the economics of breakwater size.

In order to get over these weakness of conventional slit-type breakwater, this study proposes the new concept of perforated breakwater. The variable shape of channels and slit plate are set in the caisson breakwater. The amplified wave energy is transferred to flow energy in the channel and it passes through the perforated plate. The interference of the waves on the perforated plate and the energy dissipation of the water jets issuing from the wall holes are the main hydraulic mechanism which might control the weakness.

1.2 Literature Survey

In order to investigate the characteristics of reflection and transmission waves from vertical cylinders, hydraulic model experiments have been performed by Kakuno and Liu (1993). For predicting the reflection and transmission phenomenon, analytical solutions are proposed to circular cylinders on two-dimensional cross section by Linton and Evans (1990). Analytical models for cylinders with an arbitrary cross section are developed based on the method of matched asymptotic expansions by Martin and Dalrymple (1998) and Kakuno and Liu (1993). A matched asymptotic theory of scattered wave by an array of vertical cylinders is developed to calculate reflection and transmission coefficient on small amplitude waves (Kakuno and Liu, 1993). To calculate the energy loss from flow separation at near array of cylinders as linearized form of the quadratic resistance law, they considered inertial resistance and a complex blockage coefficient related with blockage coefficient and effect of cylinders. Kakuno and Liu also determined the empirical energy loss coefficient for circular and rectangular cylinders. Kakuno et al. (1995) performed model tests for the scattering small amplitude waves on an

array of vertical cylinders, and they obtained the considerable energy dissipation result affected by flow separation near the cylinders. Kim et al. (1997) proposed an analytical model for calculating hydrodynamic forces on equally arranged vertical cylinders.

Many researchers had shown interests in interaction analysis between waves and porous structures. The analytical solutions and experimental results on an array of cylinders are applied to wave energy dissipation of slit/or perforated breakwaters. Kakuno and Oda (1986) investigated structural design to reduce wave reflection by analyzing interaction of wave-cylinder array. Dalrymple et al. (1991) developed theoretical solution of the reflection and transmission waves on porous structures using eigenfunction expansion in fluid. Kakuno et al (1992) performed hydraulic model tests for wave reflection from a perforated wall caisson on flat bottom. Park et al. (1993) investigated wave reflection from a partially perforated wall caisson breakwater on rubble mound by hydraulic model tests.

For predicting the reflection coefficient of perforated caisson breakwater, analytical models are developed. Kondo (1979) developed an analytical model based on linearized shallow water wave theory for calculating reflection coefficient of single and double perforated wall caisson breakwater with chambers. Kondo proposed the optimal width of water chamber $B/L > 0.3$, in which B is width of water chamber abd L is wave length. Fugazza and Natale (1992) developed a closed form solution for wave reflection from multi-chamber perforated wall caisson breakwater. It is applied the matching conditions of velocity and energy for each of divided region and they also proposed the optimal width of water chamber $B/L = 0.25$. Kim (1998) developed analytical model considering the perforated wall caisson breakwater and porous seabed. Each of divided region is applied matching condition of velocity and continuity pressure. Kim proposed optimal width of channel $B/L \simeq 0.22$ and optimal porosity $r = 0.25$. Massel (1993) proposed Galerkin-eigenfunction method based on extended refraction and diffraction equation. Suh and Park (1995) developed an analytical model for predict wave reflection from a perforated-wall caisson breakwater on rubble mound for obliquely incident waves. Suh (1996) more advanced the analytical model of Suh and Park (1995) from fully perforated-wall breakwater to partially perforated-wall breakwater. Suh et al (2006) also performed experiment on the partially perforated caisson breakwaters

to discuss the reflection characteristics and they proposed optimal width of water chamber $B/L \simeq 0.2$ experimentally. The similar permeable coastal structures are also variously researched. Fujita et al. (2003) had adopted L-shaped bulkhead inside the caisson of the breakwater and or seawall to get low wave reflection performance. Lee et al (2011) introduced cylindrical slit type breakwater/seawall to reduce wave reflection allowing wave transmission.

The slit caisson breakwater having the embedded channels was evaluated based on reflection characteristics by Kim et al (2014a). They were also discussed the effect of the number of embedded channel on reflections. The multi-embedded channels was shown more efficiently reducing reflected waves at multi-embedded channels than single embedded channel. Kim et al (2014b) was also proposed the influence of various shapes of the single embedded channel on reflection coefficients.

1.3 Research Objectives and Scope

The conventional perforated breakwater is required to wide width of water chamber for proper wave energy dissipation of longer wave period, and it is exposed to impact wave loads directly. Unfortunately, no alternative was proposed for solving the problems of the conventional perforated breakwater aforementioned, although a lot of study has been performed. In this study, a new concept slit(perforated) breakwater is proposed, which is having embedded channel in caisson breakwater. In the channel, the perforated plates are installed for dissipating wave energy induced by flow separations. This type of breakwater has merits compared with conventional perforated breakwater having wave chamber with slotted walls. It is easy to control the target wave condition for dissipating wave energy, because the natural characteristics of fluid in the channel are clear and simple. Also it has the high structural safety because the structural members are set under water, therefore not exposed to impact waves directly.

This dissertation consists of five chapters. In chapter 2, an analytical model for calculating wave reflection and transmission from vertical cylinders on flat bottom is represented, and it applied to slit plate of present model. The slit plate is consisted by an array of vertical rectangular cylinders. In chapter 3, the finite

element formulations are introduced applying to the present model. In chapter 4, the numerical simulation results will be discussed for applying to embedded single and multi-channels. In chapter 5, the hydraulic model tests will be discussed by comparing with numerical results and hydraulic model test results. In the present study, the numerical model is validated by comparing with hydraulic model test results and the analysis of reflection characteristics is performed for evaluating performance of this breakwater. Finally, the conclusions of present study are summarized in chapter 6.

CHAPTER 2
THEORETICAL FORMULATION

2.1 Boundary Value Problem

For the detail analysis of wave and structure interaction, it is necessary to use the complex non-linear theory. But, for efficiently evaluating the basis function of coastal structures, the fluid domain in linear potential theory is generally considered. The two dimensional numerical analysis is performed in frequency domain under the action of monochromatic waves and is based on the linear potential theory. It is assumed that the fluid is inviscid and incompressible, and its flow is irrotational in the whole fluid domain. Also incident wave height is assumed to be small and then the behaviors of water wave particles in fluid region can be described with a velocity potential Φ which satisfies the Laplace equation.

To discrete the problem domain efficiently, the required domain was divided into channel region, inner region and far field region. In the far field region, the progressive waves are periodically oscillating in the horizontal direction, and satisfy the radiation condition at infinity.

The idealized geometry of two dimensional numerical analysis is shown in Fig. 2.1. The slit caisson breakwater with resonant embedded channel is located in the constant water depth h, and related with shape parameters are shown as depth of channel inlet D, width of channel B. At the entrance of channel, the dash lines represent the slit-plate for energy dissipation. Each of divided regions are connected by matching condition, related with continuity of velocity and pressure.

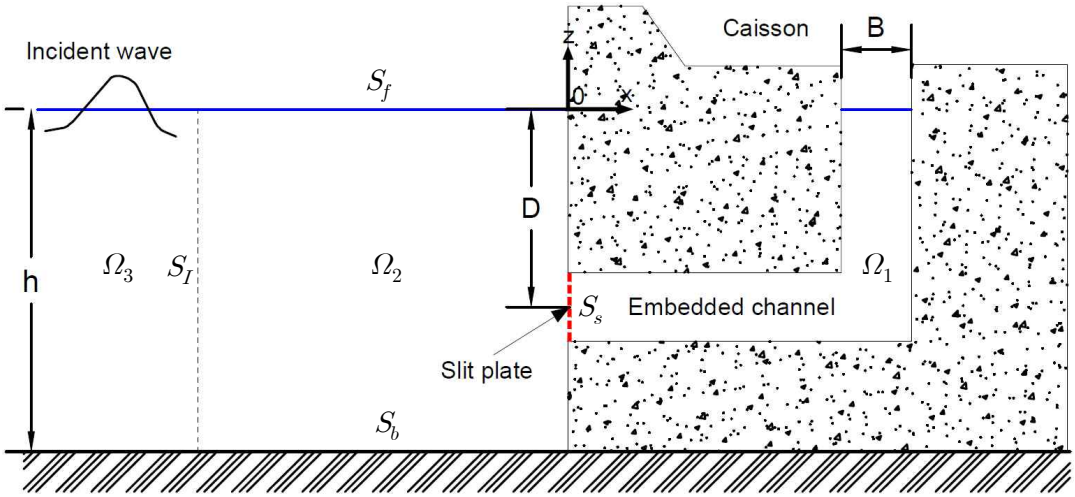

Fig. 2.1 Definition sketch of a slit caisson breakwater with a embedded resonant channel

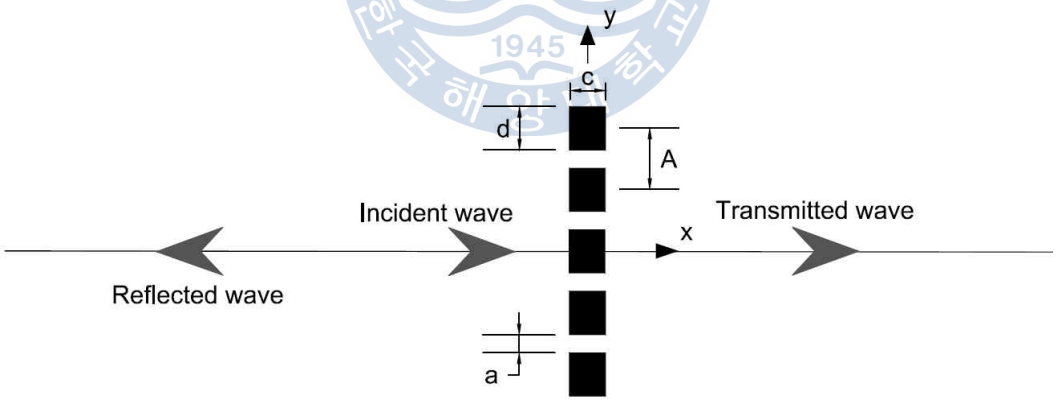

Fig. 2.2 Definition sketch of the rectangular cylinders array of the slit plate and coordinate system of plane view

Fig. 2.2 shows wave response through the vertical cylinders which have the slit width(a) and rectangular cylinder width(d). The interval of vertical cylinder has A, where $P = a/A$ is porosity of the structure.

A train of regular wave with amplitude $H/2$, and angular frequency ω, propagating toward the slit caisson breakwater with embedded resonant channel is considered as shown Fig. 2.1. A Cartesian coordinate system (x,z) with x in the direction of wave propagation and z vertically upwards from the still water level is adopted.

The boundary value problem is defined in Fig. 2.1. For efficient analysis, the wave field is divided into three region, i.e. the inner channel region Ω_1, the inner region Ω_2 and the far field region Ω_3. If the incident wave potential Φ_I is assumed to be known in the far field region, the unknown potential Φ_3, is taken to be the reflected wave potential, i.e. $\Phi_3 = \Phi_R$. In the inner field region, the unknown potential Φ_1 is taken as the sum of incident wave potential Φ_I and reflected wave potential Φ_3, i.e. $\Phi_1 = \Phi_I + \Phi_3$. In the transmitted region from vertical cylinders, Φ_2 is taken to be the transmitted wave potential, i.e. $\Phi_2 = \Phi_T$. This model is evaluated by the reflection characteristics of two dimensional wave field at the front side.

2.2 Fluid Domain

Assuming incompressible, inviscid fluid and irrotational flow, the velocity potential $\Phi(x,z,t)$ for the monochromatic wave propagating over the constant water depth h, with the angular frequency ω, and incident wave height H, can be expressed as:

$$\Phi(x,z,t) = \frac{gH}{2\omega}\phi(x,z)\frac{\cosh k(z+h)}{\cosh kh}e^{-i\omega t} \tag{2.1}$$

where g = gravitational acceleration, $i = \sqrt{-1}$, and k = wave number. These components have to satisfy the dispersion relation equation.

$$\omega^2 = gk\tanh kh \tag{2.2}$$

The motion of fluid particles can be described by a velocity potential,

$$\nabla^2\Phi(x,z,t) = 0 \tag{2.3}$$

in which $\nabla^2 = \partial^2/\partial x^2 + \partial^2 z/\partial z^2$. In addition, the wave height is assumed to be sufficiently small for linear wave theory to be applied. Consequently, $\Phi(x,z,t)$ is subject to the usual boundary conditions at the free surface (S_f) and impermeable surface (S_b) as follows:

$$\frac{\partial\Phi}{\partial z} = \frac{\omega^2}{g}\Phi \qquad \text{on } S_f \tag{2.4}$$

$$\frac{\partial\Phi}{\partial n} = 0 \qquad \text{on } S_b \tag{2.5}$$

in which impermeable surface (S_b) is applied to the surface of structure and seabed.

The velocity potential Φ is harmonic and made up of components associated with the incident wave and/or scattered wave, i.e. reflected or transmitted.

$$\Phi_1 = \Phi_I + \Phi_R = (\phi_I + \phi_R)e^{-i\omega t} \tag{2.5}$$

$$\Phi_2 = \phi_T e^{-i\omega t} \tag{2.6}$$

in which ϕ_I, ϕ_R and $\phi_T =$ complex-valued amplitude for incident and scattered wave potential (reflected and transmitted waves) generated from the slit plate. The matching boundary condition on the interface between the near and far field region S_I can be expressed.

$$\frac{\partial \Phi_1}{\partial n} = -\frac{\partial(\Phi_I + \Phi_R)}{\partial n} \quad \text{on } S_I \tag{2.7}$$

The velocity potential ϕ_T associated with the scattered waves, i.e. reflected generated from the slit plate must satisfy the Sommerfeld radiation condition (Sommerfeld, 1949) at infinity

$$\lim_{r\to\infty}\left(\frac{\partial}{\partial r} - ik\right)\phi_T = 0 \tag{2.8}$$

in which $r = |x|$, $x =$ a horizontal distance wave generating source and $k =$ wave number of progressive wave component.

2.3 Energy Dissipation at Slit Plate

The potential $\phi_j(x,z)$ $(j=1,2)$ satisfy the matching conditions at the vertical cylinders, the velocity continuity equation at vertical cylinders is follow as:

$$\frac{\partial \phi_1}{\partial x} = \frac{\partial \phi_2}{\partial x} \tag{2.9}$$

in which subscripts $j=1$ and 2 are left and right side from the slit; $\phi_1 =$ left side of fluid region and $\phi_2 =$ right side of fluid region. Its vertical rectangular cylinders array are consisting the slit plate.

The matching condition (Mei, 1989) denoting the continuity of pressure at the separated fluid region by vertical cylinders of the slit plate is follow as:

$$\frac{p_1}{\rho_f} = \frac{p_2}{\rho_f} + \frac{1}{2}\alpha u_2 |u_2| + \int_l \frac{\partial u_2}{\partial t} dl \tag{2.10}$$

in which $p = -\rho_f Re[\partial \Phi / \partial t]$, $\rho_f =$ density of the water, $u_2 = Re[\partial \Phi / \partial x] = \gamma u_1$ is the mean velocity away from the slit plate, u_1 = velocity at the slit plate and α = energy loss coefficient. The symbol $Re[\bullet]$ represents the real part of a complex value. The energy loss coefficient α, from flow separation phenomenon through vertical rectangular cylinders is derived from the head loss coefficient for the plate orifice formula (Mei, 1989)

$$\alpha = \left(\frac{1}{r C_c} - 1 \right)^2 \tag{2.11}$$

in which r = the porosity of rectangular cylinders array of the slit plate, C_c = the empirical contraction coefficient at the slit plate. Hattori (1972) proposed that the contraction coefficient range from 0.4 to 0.75 for rectangular cylinders. Kim (1998) used C_c=0.70 for the rectangular cylinders and C_c=0.95 for the circular cylinders, using the comparison of hydraulic experiment and numerical results.

In the (2.10), l is the length of the jet flowing through the vertical cylinders and represents the inertial resistance at the vertical cylinders. Suh (1996) compared the Kakuno and Liu's (1993) model and Suh and Park's (1995) model. The length of the jet flow l follow as:

$$l = 2C' \tag{2.12}$$

in which C' is a blockage coefficient which is defined as a function of geometrical properties of an array of the vertical cylinders and is independent of the wave characteristics.

For rectangular cylinders, C' is given as (Taylor, 1973; Kakuno and Liu, 1993; Kim, 1998; Suh et al, 2006)

$$C' = \frac{c}{2}\left(\frac{1}{r} - 1\right) + \frac{A}{\pi}\left[1 - \log(4r) + \frac{1}{3}r^2 + \frac{281}{180}r^4\right] \tag{2.13}$$

in which c = thickness of the rectangular cylinder for wave propagating direction, A = the width of the rectangular column and r = the porosity of rectangular cylinders array of the slit plate $r = a/A$. When the opening ratio r is lower than 0.6, the blockage coefficient C' is applicable in (2.13). In the present study, the slit plate in front of channel is considered by the array of rectangular cylinders.

For the effectively analysing the problems, the third term of right side in (2.10) is simplified assuming that the acceleration of water particle on jet flow is constant, and the second non-linear term of right side in (2.10) is linearized using Lorentz's transformation and averaging power over depth.

$$\int_{-h}^{0} \frac{1}{2} \alpha u_2 |u_2| \cdot u \, dz = \int_{-h}^{0} \beta u_2 \cdot u_2 \, dz \tag{2.14}$$

in which β = linearized dissipation coefficient, is obtained as:

$$\beta = \frac{\int_{-h}^{0} \frac{1}{2} \alpha u_2 |u_2| \cdot u_2 \, dz}{\int_{-h}^{0} u_2 \cdot u_2 \, dz} \tag{2.15}$$

In the Eq. (2.10), linearizing the nonlinear head-loss term and assuming that the acceleration of water particle on jet flow is constant, the matching condition for the continuity of pressure at slit plate (Suh and Park, 1995) can be expressed:

$$\frac{\partial \phi_1}{\partial x} = \frac{1}{\left(l + \frac{i\beta}{\omega} \right)} \left[\phi_2 - \phi_1 \right] \tag{2.16}$$

2.4 Motion of Fluid in Channel

The motion of fluid in the channel region may be idealized as a single degree of freedom system as shown in Fig. 2.3. The equation of fluid motion can be expressed as:

$$M_c\ddot{z}_c + k_c z_c = F_c \tag{2.17}$$

in which $\ddot{z}_c$, z_c = acceleration and displacement of the fluid in the channel, respectively; the mass of fluid in the channel, $M_c = \rho B L_c$, the restoring coefficient of oscillating fluid in the channel, $k_c = \rho g B$, the total force from fluid motion, $F_c = p_c B$, and in these terms, L_c = length of the channel centerline, p_c = hydrodynamic pressure of incident and reflected waves at center of channel inlet.

Assuming harmonic motion, the complex-valued amplitude of $\overline{z_c}$ can be obtained as:

$$\overline{z_c} = \frac{\overline{F_c}}{-\omega^2 M_c + k_c} \tag{2.18}$$

in which $\overline{F_c}$ = complex-valued amplitude of F_c. The natural frequency from the motion equation is $\omega_n = \sqrt{k_c / M_c}$, then the natural period of fluid in the channel is obtained as:

$$T_n = 2\pi\sqrt{\frac{L_c}{g}} \tag{2.19}$$

The natural period for a simple pendulum at the right side of Fig. 2.3 depends on only the center length of the channel L_c and gravitational field strength.

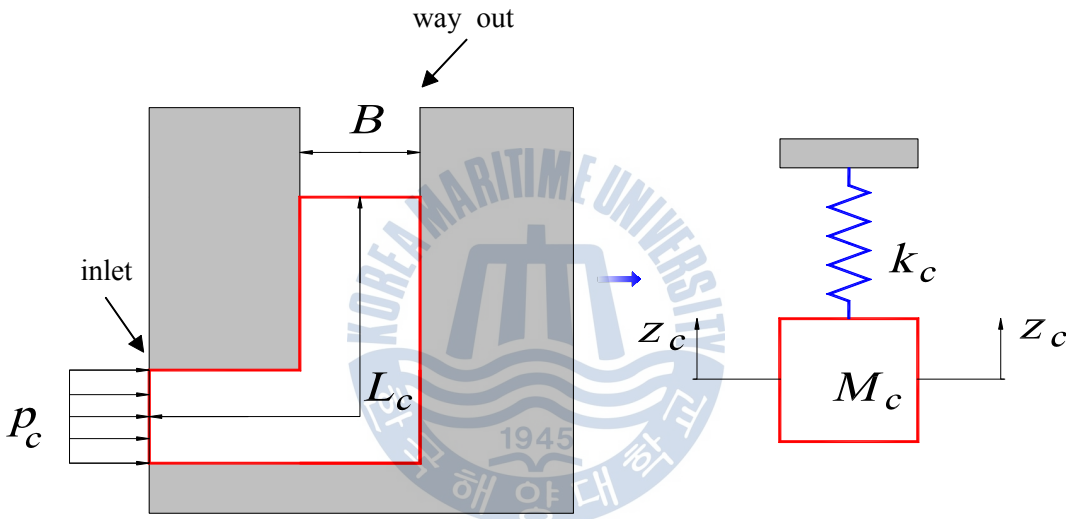

Fig. 2.3 Idealized single degree of freedom system of fluid in the embedded channel

CHAPTER 3

FINITE ELEMENT FORMULATION

3.1 General

To discretize the problem domain efficiently, the analyzed domain was divided into three regions. The conventional finite elements are applied to channel fluid region and inner fluid region. The other region is a far field region that is represented as infinite elements. The shape function of the infinite element is derived from the behaviors of the progressive wave and the first evanescent mode components in the analytical boundary series solutions (Park et al., 1991). The infinite element with periodically oscillated shape function in the horizontal direction is used satisfy the radiation condition at infinity. In order to simulate the energy losses at the slit plate, the energy dissipation is considered by flow separation at slit plate between channel fluid region and inner region. The matching conditions were introduced on the interface boundary of there two regions, i.e. the continuity conditions of velocity and pressure at the slit plate. These matching conditions may be expressed on the joint elements connecting both regions.

3.2 Discretization of Fluid Domain

To discretize the problem in the standard finite element manner, it is necessary to describe the unknown potential ϕ_j in terms of the complex-valued nodal vector ϕ_j^e and the shape function vector N_ϕ as follows.

$$\phi_j = N_\phi^T \phi_j^e \tag{3.1}$$

The subscript j in Eq. (3.1) denotes the inner reflected region for $j=1$, the channel region inside of caisson for $j=2$, the outer reflected region for $j=3$.

Using Galerkin's technique, the boundary value problem can be reformulated as integral equations for the element matrices. The element contribution to the system of equations is given by

$$R^e = \int_{\Omega_j^e} N[\nabla^2 \phi_j] d\Omega_j^e \tag{3.2}$$

in which N is the vector of element shape functions. Using the technique of integration by parts and Eqs. (2.4), (2.5), (2.8) and (2.18), the system equations can be obtained as following simultaneous equations:

$$\sum_e K_{\phi\phi} \phi_j^e = \sum_e f_\phi^e \tag{3.3}$$

in which

$$K_{\phi\phi} = \int_{\Omega^e} \left(\frac{\partial N_\phi}{\partial x} \frac{\partial N_\phi^T}{\partial x} + \frac{\partial N_\phi}{\partial z} \frac{\partial N_\phi^T}{\partial z} \right) d\Omega^e - \int_{S_f^e} \frac{\omega^2}{g} \partial N_\phi \partial N_\phi^T dS_f^e - \int_{S_J^e} \frac{1}{\left(l + \frac{i\beta}{\omega} \right)} N_\phi N_\phi^T dS_J^e \tag{3.4}$$

$$f_\phi^e = \int_{S_I^e} N_\phi \frac{\partial \phi}{\partial n} dS_I^e \tag{3.5}$$

in which the superscript e denotes that the corresponding integrations are taken over a single element only.

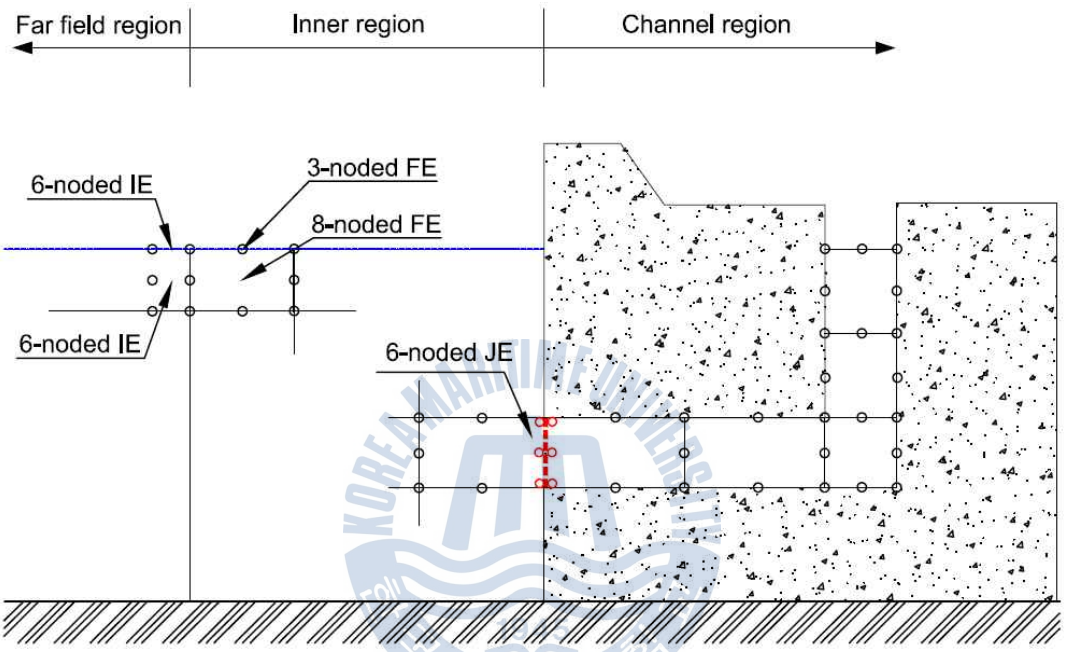

FE = Finite Element

IE = Infinite Element

JE = Joint Element

Fig. 3.1 Finite element grid for wave-structure interactions

3.2.1 Finite Element Region

To discretize the fluid domain efficiently, the channel region Ω_1, and inner region, Ω_2, are descretized using conventional iso-parametric elements, i.e. 8-noded quadrilateral elements and 3-noded line elements as shown in Fig. 3.1. The element coordinates are defined in Fig. 3.2. The Lagrange polynomial is used as the shape functions for iso-parametric elements.

(a) 8-noded finite element $(-1 \le \xi,\ \eta \le 1)$

$$N_\phi = \begin{bmatrix} N_1 \\ N_2 \\ N_3 \\ N_4 \\ N_5 \\ N_6 \\ N_7 \\ N_8 \end{bmatrix} = \begin{bmatrix} -(1-\xi)(1-\eta)(1+\xi+\eta)/4 \\ (1-\xi^2)(1-\eta)/2 \\ -(1+\xi)(1-\eta)(1-\xi+\eta)/4 \\ (1+\xi)(1-\eta^2)/2 \\ -(1+\xi)(1+\eta)(1-\xi-\eta)/4 \\ (1-\xi^2)(1+\eta)/2 \\ -(1-\xi)(1+\eta)(1+\xi-\eta)/4 \\ (1-\xi)(1-\eta^2)/2 \end{bmatrix} \tag{3.6}$$

(b) 3-noded finite element $(-1 \le \xi \le 1)$

$$N_\phi = \begin{bmatrix} N_1 \\ N_2 \\ N_3 \end{bmatrix} = \begin{bmatrix} -\xi(1-\xi)/2 \\ (1-\xi^2) \\ -\xi(1+\xi)/2 \end{bmatrix} \tag{3.7}$$

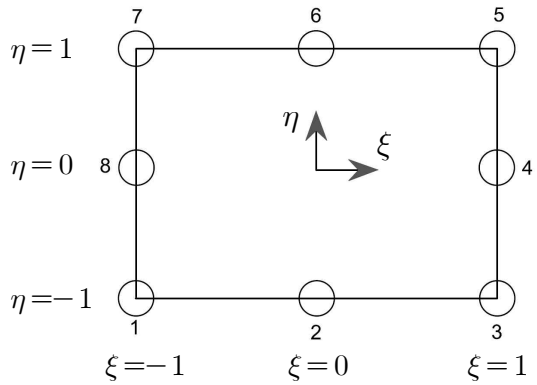

(a) 8-noded FE

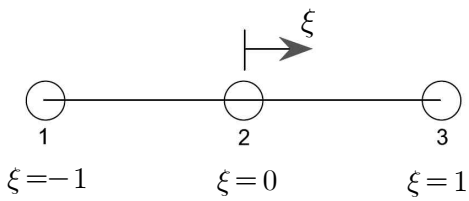

(b) 3-noded FE

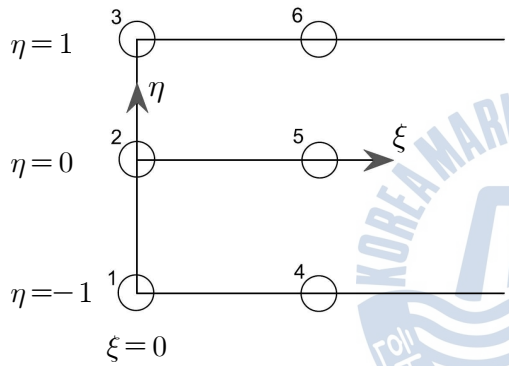

(c) 6-noded IE

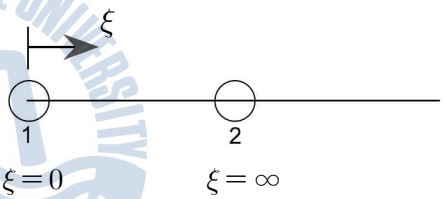

(d) 2-noded IE

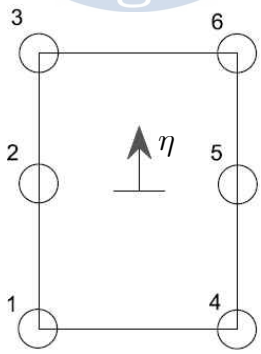

(e) 6-noded JE

Fig. 3.2 Definition of element coordinates

The 8-noded quadrilateral element is for modeling the governing equation, while the 3-noded line element is for modeling the boundary condition.

The inner reflected region and channel region are connected using 6-noded joint elements. Using the matching condition (2.10) at slit plate (S_s), the system matrix for joint element can be constructed as

$$K_{\phi\phi} = -\int_{S_S^e} \frac{1}{\left(l+\frac{i\beta}{\omega}\right)} N_\phi N_\phi^T dS_S^e$$

$$= \frac{1}{\left(l+\frac{i\beta}{\omega}\right)} \begin{bmatrix} K_{\eta\eta} & -K_{\eta\eta} \\ -K_{\eta\eta} & K_{\eta\eta} \end{bmatrix} \tag{3.8}$$

in which $K_{\eta\eta}$ is 3×3 matrix defined as

$$K_{\eta\eta} = \int_{z^e} N(\eta) N^T(\eta) dz \tag{3.9}$$

in which $N(\eta) =$ Lagrange shape function vector.

$$N(\eta) = \begin{bmatrix} -\eta(1-\eta)/2 \\ (1-\eta^2) \\ \eta(1+\eta)/2 \end{bmatrix} \tag{3.10}$$

The system matrices of Eqs. (3.4) and (3.5) for an element are constructed using the Gaussian quadrature.

3.2.2 Infinite Element Region

In order to model the scattered wave behaviors in the far field region, Ω_3, two type of infinite elements (IE), which have been developed by Park et al. (1991), were used. They are the 6-noded infinite element for discretizing the fluid domain and 2-noded infinite element for modeling the free surface boundary condition in the outer region. As shown in Fig. 3.1, the outer region is modeled using these elements with the shape functions derived from the analytical boundary series solutions such as

(a) 6-noded infinite element ($0 \le \xi \le \infty,\ -1 \le \eta \le 1$)

$$N_\phi = \begin{bmatrix} M_i(\xi) & N(\eta) \\ M_o(\xi) & N(\eta) \end{bmatrix} \tag{3.11}$$

(b) 2-noded infinite element ($0 \le \xi < \infty$)

$$N_\phi = \begin{bmatrix} M_i(\xi) \\ M_o(\xi) \end{bmatrix} \tag{3.12}$$

in which $M_{i(\xi)}$ and $M_{o(\xi)}$ = shape function in the horizontal direction as

$$\begin{bmatrix} M_i(\xi) \\ M_o(\xi) \end{bmatrix} = F^T \begin{bmatrix} f_o(\xi) \\ f_1(\xi) \end{bmatrix} \tag{3.13}$$

in which $f_o(\xi)$ and $f_1(\xi)$ represent the asymptotic behavior of the progressive and the first evanescent wave components in the horizontal directions, respectively, and F is the 2×2 coefficient matrix associated with those wave components, which are given by

$$f_o(\xi) = e^{ik(\xi+r_i)-\epsilon_d\xi} \tag{3.14}$$

$$f_1(\xi) = e^{-k_1(\xi+r_i)} \tag{3.15}$$

$$F = \begin{bmatrix} e^{ikr_i} & e^{-k_1 r_i} \\ e^{ikr_o} & e^{-k_1 r_o} \end{bmatrix}^{-1} \tag{3.16}$$

and ϵ_d = the artificial decaying parameter ($0 < \epsilon_d \ll k$), k_i = the wave number for the first evanescent mode, r_i and r_o = the distance to the inner and outer nodes of the infinite element from the origin. Without introducing the artificial decaying parameter, ϵ_d, the system matrices for the infinite elements cannot be formulated, since integrated value in the $\xi-$direction does not exist.

$M_i(\xi)$ and $M_o(\xi)$ in Eq. (3.13), except for ϵ_d, have been derived from the behaviors of the progressive wave and the first evanescent mode component in the analytical boundary series solutions such as (see. Appendix A.1)

$$\phi_j \approx a_1 e^{ikr} + b_1 e^{-k_1 r} \tag{3.17}$$

The above shape functions satisfy the radiation condition (2.8) at infinity.

Since the shapes of the infinite elements are restricted as shown in Fig. 5.3, the system matrices for the element can be constructed by performing the integrations in the $\xi-$ and $\eta-$directions, separately. In this study, the integration in the infinity direction ($\xi-$direction) is performed analytically. Then, the system matrices for the infinite elements can be constructed as Park et al. (1991).

(a) 6-noded infinite element

$$K_{\phi\phi} = \begin{bmatrix} A_{11}K_{\eta\eta} + B_{11}K_{\eta'\eta'} & A_{12}K_{\eta\eta} + B_{12}K_{\eta'\eta'} \\ A_{12}K_{\eta\eta} + B_{12}K_{\eta'\eta'} & A_{22}K_{\eta\eta} + B_{22}K_{\eta'\eta'} \end{bmatrix} \tag{3.18}$$

(b) 2-noded infinite element

$$K_{\phi\phi} = -\frac{\omega^2}{g}\begin{bmatrix} B_{11} & B_{12} \\ B_{12} & B_{22} \end{bmatrix} \tag{3.19}$$

in which A_{ij} and B_{ij} are the complex valued coefficients associated with the integration of infinite direction (see Appendix A.2), and $K_{\eta'\eta'}$ is 3×3 matrix defined as

$$K_{\eta'\eta'} = \int_{z^e} \frac{\partial N}{\partial z}\frac{\partial N^T}{\partial z} dz \tag{3.20}$$

Gaussian quadrature is used for the integrations in Eq. (3.20) in the η-direction.

In the inner region, the unknown nodal potential values denote the total velocity potential including the incident wave potential, ϕ_I, and the reflected wave potential, ϕ_3 generated from the slit-plate caisson with embedded resonant channel. However, in the outer region, ϕ_3 is only unknown, while ϕ_I is given. Therefore, those effects should be included in the exciting force vector of Eq. (3.5) as

$$f_{\phi}^{e} = -\int_{S_I^e} N_{\phi} \frac{\partial \phi_I}{\partial n} dS_I^e + K_{\phi\phi} \phi_I^e \tag{3.21}$$

in which $K_{\phi\phi}$ = the system matrix for the infinite element and ϕ_I^e = the nodal potential vector of the incident wave for the corresponding nodal points.

CHAPTER 4

NUMERICAL RESULTS and DISCUSSIONS

4.1 General

The incident waves are differently reflected from the structure to the ocean. The reflected waves are formed to standing waves at near field of structures. In general, the shape of coastal structures critically affect to reflected waves. In this study, it is analyzed that the embedded channels in breakwater is affected to reflected waves. For analysis of reflection characteristics about slit caisson breakwater with embedded resonant channels, various channel shapes are applied to numerical model. The designed slit caisson breakwater is on the bottom at the constant water depth $h = 11.25m$. The channel is embedded in the slit caisson breakwater, and consisted by vertical and horizontal regions. The channel inlet is set on the horizontal region under water surface and the way out of embedded channel is vertically arranged. The width of channel B is constant. The length of passing line at center of channel is related with resonant period of channel, Eq. (2.29). The slit plate for wave energy dissipation is located in front side of channel inlet, and the vertical rectangular column is applied to vertical slit plate. The conceptual model of slit caisson breakwater with a embedded resonant channel is shown in Fig. 4.1.

In this analysis, channel region (Ω_1) and the inner region (Ω_2) are discretized to finite element (FE), and the far field region (Ω_3) is modeled using infinite element (IE). The element grid of slit caisson breakwater with a embedded resonant channel is presented in Fig. 4.2. The channel region (Ω_1) and the inner region (Ω_2) are matched using joint element (JE).

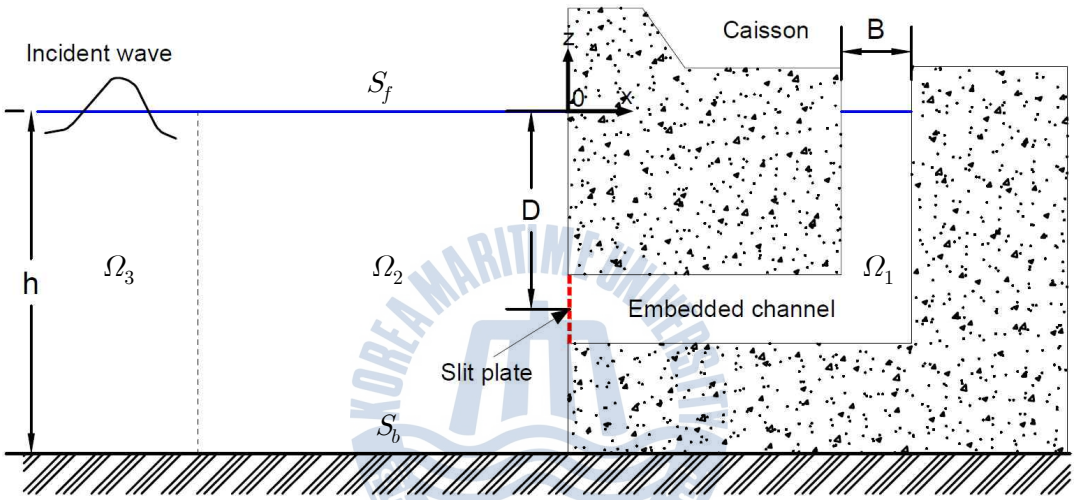

Fig. 4.1 Definition sketch of a slit caisson breakwater with an embedded resonant channel

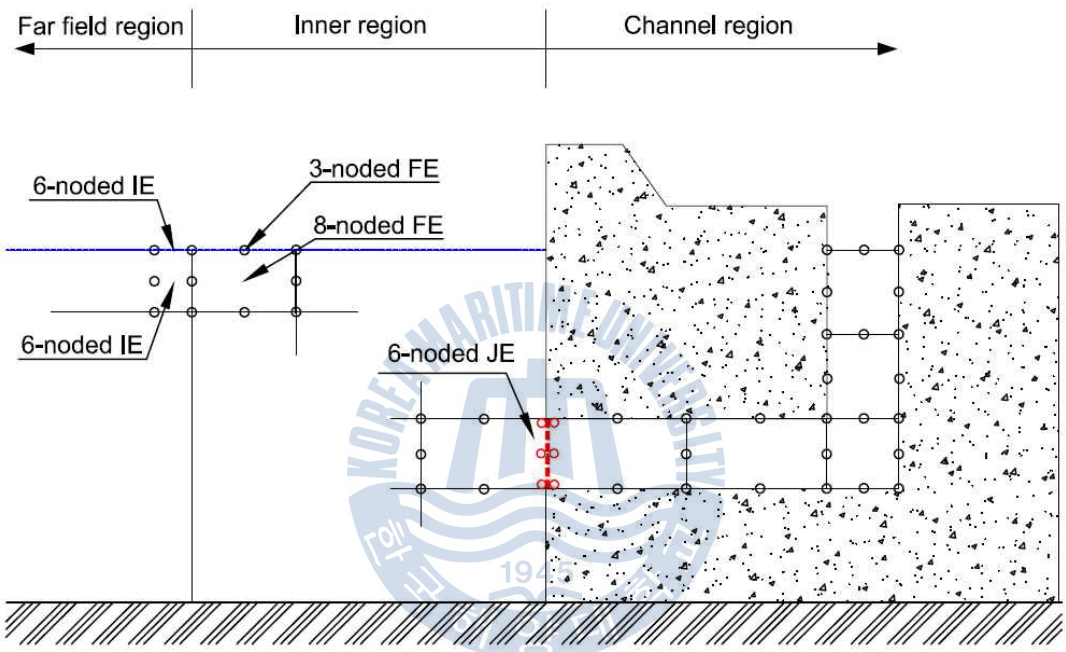

FE = Finite Element

IE = Infinite Element

JE = Joint Element

Fig. 4.2 Element grid for wave-structure interactions including finite, infinite and joint meshes

The wave energy dissipation at the slit plates are influenced by porosity (opening ratio) of the slit plate. The porosities of the slit plate are considered from 0.2 to 0.6 with interval $\Delta r = 0.05$. The properties of the slit plates are shown in the Table 4.1. In the Table 4.1, r is the porosity (opening ratio) of the slit plate, α is the energy loss coefficient of the slit plate and l is the length of the jet flow. Also the C_c is the empirical contraction coefficient at the slit wall, its value was proposed by kim (1998).

Table 4.1 Properties for the slit plate and coefficients related to energy loss due to flow separation

P $\left(= \frac{a}{A}\right)$	α $\left(= \left[\frac{1}{C_c P} - 1\right]^2\right)$	l $[m]$	Remarks
0.10	176.51	3.88	
0.15	72.66	2.55	
0.20	37.73	1.87	
0.25	22.22	1.44	
0.30	14.15	1.16	$C_c = 0.7$
0.35	9.50	0.95	
0.40	6.61	0.78	$d = 0.375$m
0.45	4.73	0.66	
0.50	3.45	0.55	
0.55	2.55	0.47	
0.60	1.91	0.40	

4.2 Embedded Single Channel Case

In order to investigate the influence of shapes of a embedded channel on reflection coefficient, the reflection characteristics are analyzed for two parameters. One is the depth of channel inlet, the other is width of channel.

4.2.1 Influence of depth of channel inlet

In order to investigate influence of an embedded channel inlet on reflection characteristics, the three of embedded channels having same width are applied to analysis. The embedded channels are located in different water depth and each of them are named by sequence from upper channel(A) to lower channel(C). Each of the channels have different natural period related with channel length, therefore the reacting incident wave period is different. For properly comparing the results, reflection coefficient is represented as a function of normalized period wave T_w/T_{ch} in which T_w is incident wave period and T_{ch} is natural period of channel. The analysis are performed in various incident wave periods $T_w/T_{ch}=0.5\sim2.0$ and porosities of slit plate $r=0.1\sim0.6$. In Fig. 4.3, the single embedded channels are set to different shape as depth of channel inlet D, length of channel L_c. Each of the channels have a same width, B=1.875m. These shape parameters are shown in Table 4.2.

Table 4.2 Shape parameters of an embedded single channel

Channel	D [m]	L_c [m]	T_n [sec]	Remarks
A	5.0625	13.875	7.472	$B=1.875$m
B	7.3215	18.375	8.599	
C	9.5625	22.875	9.595	

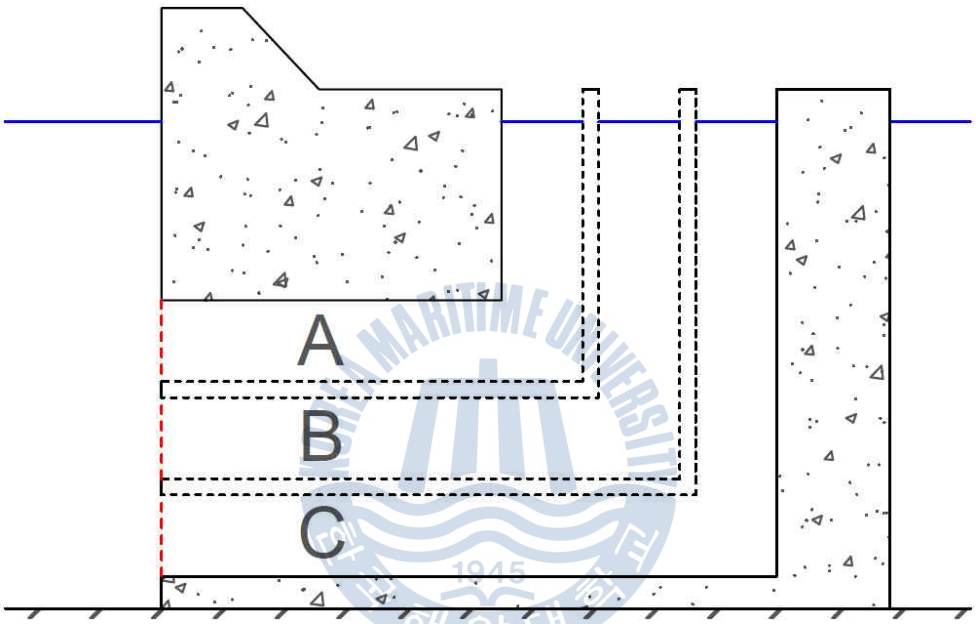

Fig. 4.3 Conceptual design of a slit caisson breakwater with the embedded channels

The element meshes for fluid region are shown in Fig. 4.4 for the slit caisson with an embedded single channel. Fig. 4.4 shows the 8-noded iso-parametric element used for discretizing the entire inner fluid region and far field region discretized by infinite element.

The meshes are consisted by finite elements and infinite elements. It is used for discretizing the fluid region. To proper analysis, meshes satisfied the minimum limit number of elements. Minimum number of element for discretizing the fluid region per a wave length are 12 for channel A, 14 for channel B and 16 for channel C in horizontal direction, which is enough for interpolation of wave potential behaviors. In general, horizontal length of the numerical water flume should be longer than incident wave length for properly formed incident wave in the numerical water flume. Furthermore, the minimum number of element for discretizing the fluid region per a wave length is 4 with quadratic elements in horizontal direction, which is enough for interpolation of wave potential behaviors. The mesh conditions of each cases are presented in Table 4.3.

Table 4.3 Mesh conditions of a slit caisson breakwater with an embedded single channel cases

Channel	A	B	C
No. of Finite Elements	595	569	511
No. of Infinite Elements	25	21	17
No. of nodes	2027	1893	1698

(a) channel A

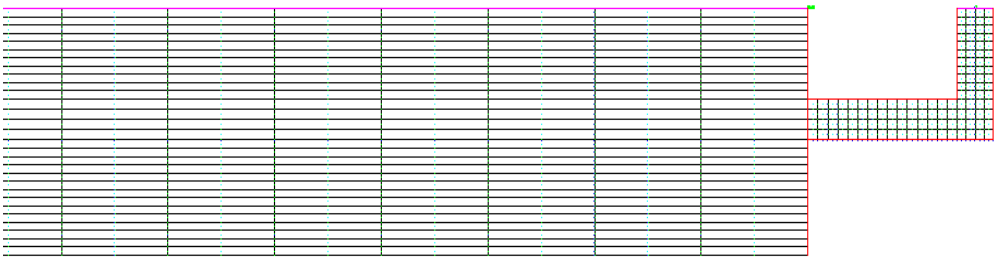

(b) channel B

(c) channel C

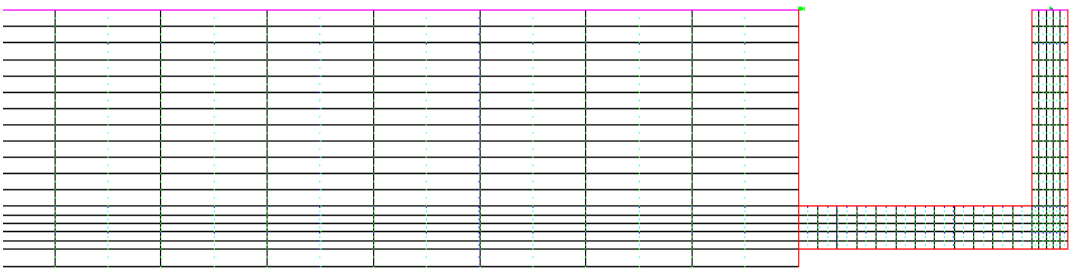

Fig. 4.4 Finite element meshes of the slit caisson breakwater with an embedded single channel

For the evaluating reflection characteristics of a slit caisson breakwater with an embedded resonant channel, reflection coefficient is represented by normalized wave period T_w/T_{ch} and porosity r in Fig. 4.5. In this figure, reflection coefficients are shown considering the porosity $r=0.2$, 0.4 and 0.6. Each of the embedded single channel cases, the minimum reflection coefficient K_R is commonly appeared at normalized wave period $T_w/T_{ch} \simeq 1$. It means that the wave energy is properly dissipate by resonant mode of fluid in the channel at near the designed natural period of embedded channel.

The porosity of slit plate r is affecting to reduction of reflection coefficient. The minimum reflection coefficient $K_{R_{\min}}$ is appeared at near $r=0.6$, and it is appeared at narrow band of incident wave period. At the porosity $r=0.2$, reduced area of reflection coefficient is more broadly spread than $r=0.6$. It is shown that the flow into the channel is properly formed at the large porosities.

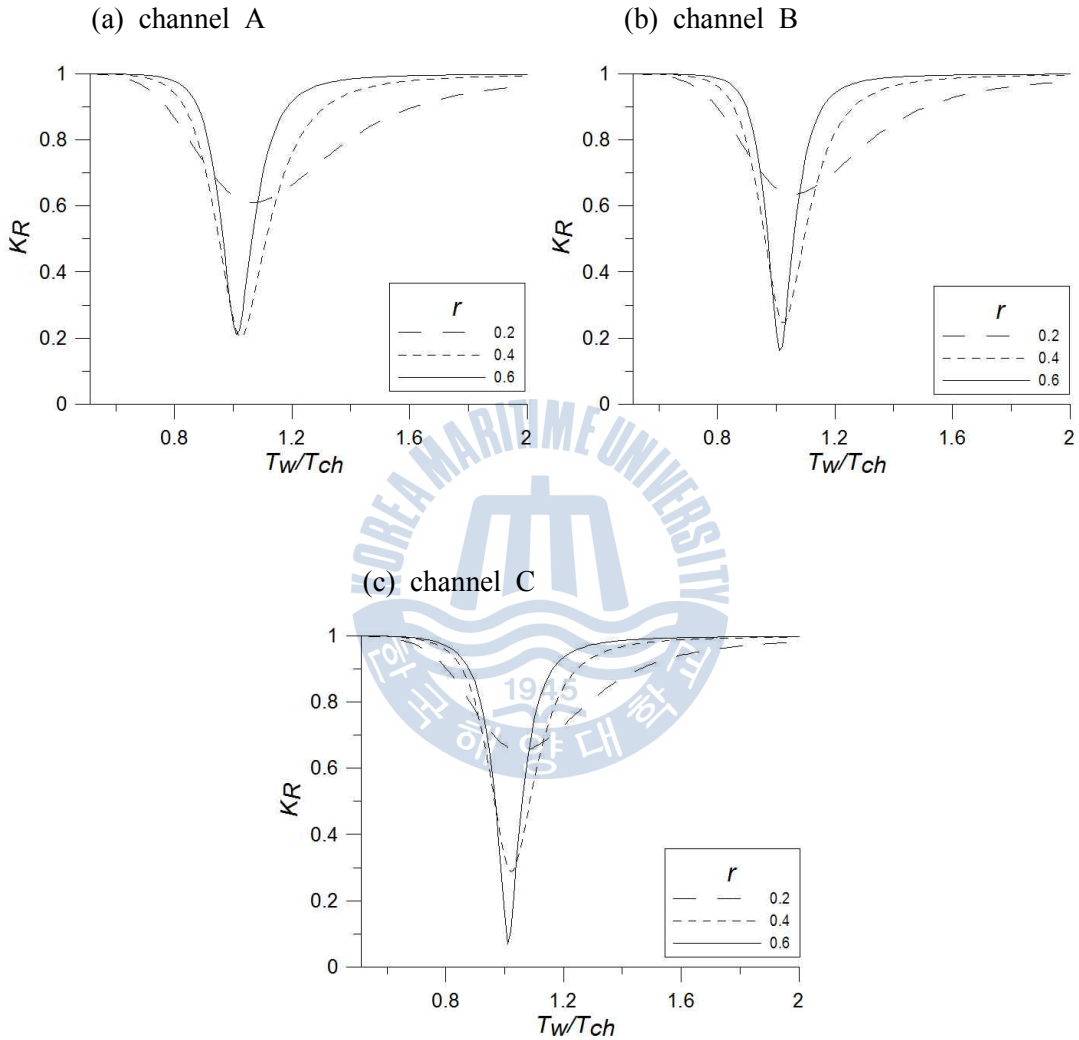

Fig. 4.5 Reflection coefficient K_R of slit caisson breakwater with an embedded single channel (A, B, C)

The effects of the changing depth of the channel inlet on reflection characteristics are analyzed in detail using contour plot of reflection coefficients. The contour of reflection coefficients are shown in Fig. 4.6 and these are expressed by using the porosities and normalized wave periods. The environmental conditions are considered as water depth $h = 11.25m$, wave height $H = 0.75m$ and normalized wave period $T_w / T_{ch} = 0.5 \sim 2.0$.

As expected, the reflection coefficient approaches to 1.0 (perfect reflection) as r goes to near zero (solid wall). The proper energy dissipation meaning of $K_R < 0.2$ is occur at the $T_w / T_{ch} \simeq 1$. It is appeared at several porosities that means the optimum porosity and their range. The optimum porosities are differently represented for each channels at contour plots in Fig. 4.6 (a), (b) and (c). The band of optimum porosities are A(r=0.4~0.55), B(r=0.45~0.6) and C(r=0.45~0.6). The wave period band of reduced K_R is more spread at the low porosity of channel A. The trend of reduced band of reflection coefficient are similar at $r > 0.3$.

In real sea state, the waves contain a lot of individual waves relating with different periods. Therefore, the evaluation of wave energy dissipation in band of interesting periods is necessary for proper design.

(a) channel A

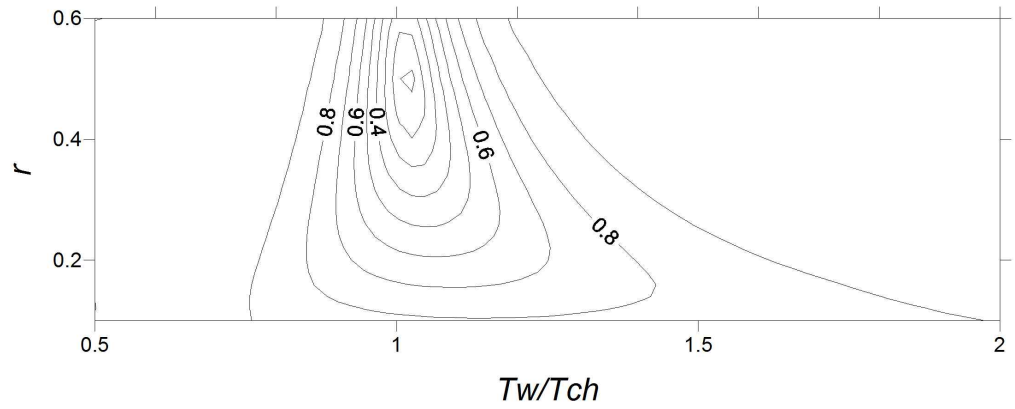

(b) channel B

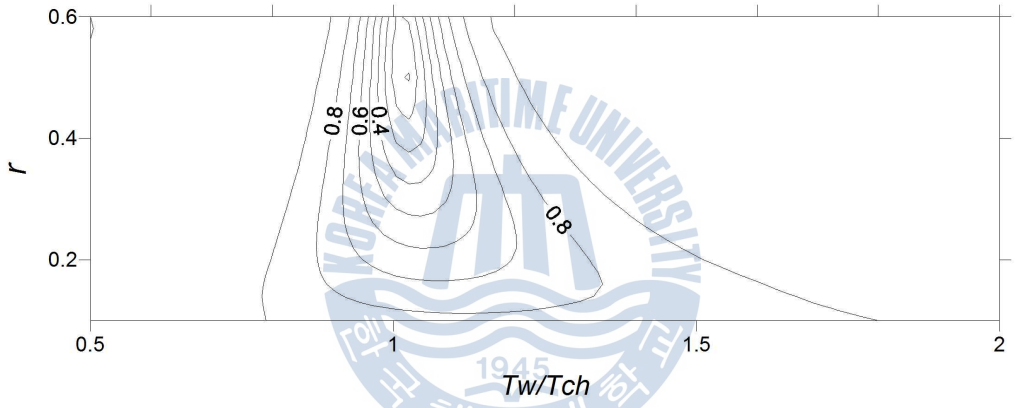

(c) channel C

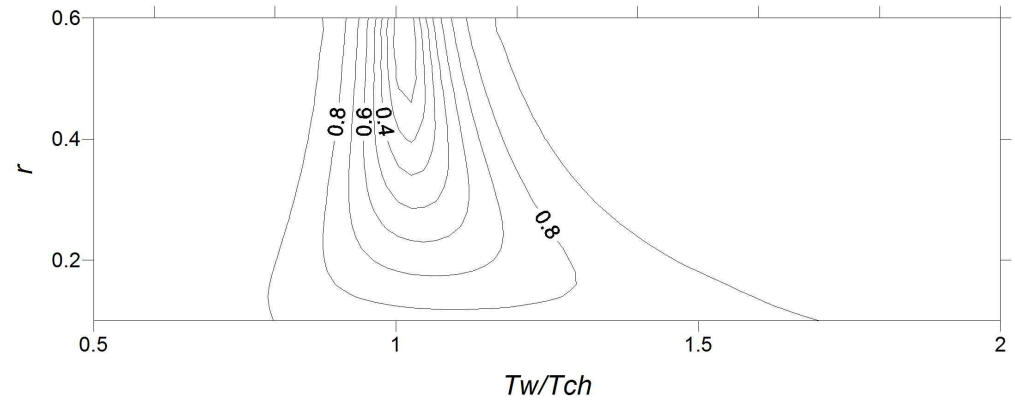

Fig. 4.6 Contour plot of reflection coefficient K_R of slit caisson breakwater with an embedded single channel (A, B, C)

The energy dissipation related with resonant mode in the embedded channel is expressed to minimum reflection coefficient $K_{R_{\min}}$ in Fig. 4.7(a). This data is based on the results of Fig. 4.6. For evaluating the effect of porosity, the porosities are considered as between 0.1 and 0.6 with interval $\Delta r = 0.05$. The minimum reflection coefficient is appeared at the $r = 0.5$ (channel A and B) and $r = 0.55$ (channel C).

The wave period of minimum reflection coefficient is defined as resonant period and it is represented in Fig. 4.7(b). The resonant mode is appeared at more longer wave period than natural period of channel $T_w / T_{ch} > 1$. It means that using embedded channel and slit plate can control energy dissipation for longer wave period than natural period of channel. This phenomenon is more shifted to longer wave period $T_w / T_{ch} = 1.11 \sim 1.15$ at low porosity $r = 0.1$.

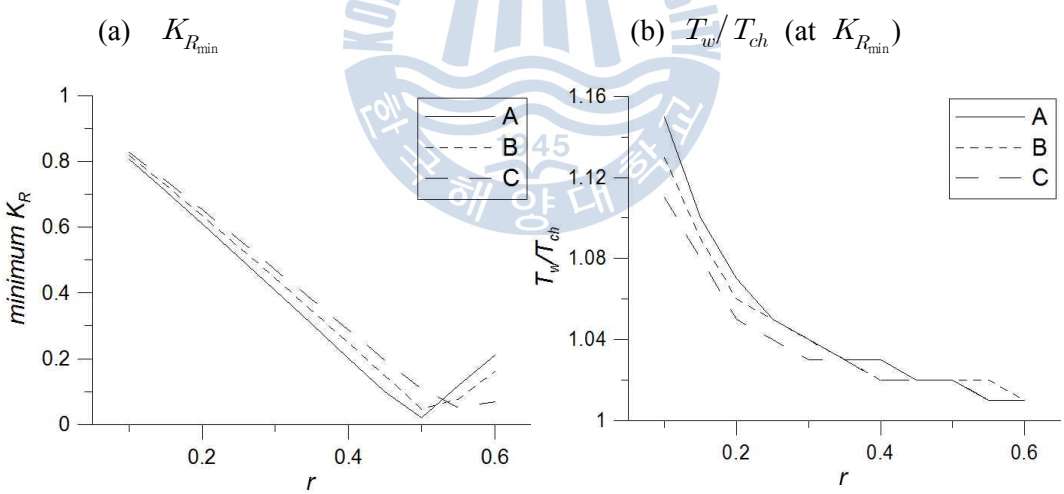

Fig. 4.7 Minimum reflection coefficient $K_{R_{\min}}$ and normalized wave period of resonant mode T_w / T_{ch} of slit caisson breakwater with an embedded single channel (A, B, C)

The inlet of channel C is relatively farther from water surface, so the wave orbital motion and flow into the channel are relatively smaller than channel A and B near water surface. For this reason, the minimum reflection coefficient is appeared more wide porosity. However, the effect of depth of channel inlet is small. Because the numerical water flume is finite water region by the relation of water depth and wave length $0.05 < h/L < 0.50$, so the water particle has flat orbital motion in horizontal direction. So, these three of single channel cases (A, B, C) show the very similar tends of reflections.

4.2.2 Influence of channel width

In order to investigate influence of an embedded channel width on reflection characteristics, the variable width of an embedded channels are applied to analysis $B/L_c = 0.1 \sim 0.3$ in which the centerline length of an embedded channel is constant $L_c = 18.75m$. The embedded channel has a same natural period $T_{ch} = 8.687\,\mathrm{sec}$ and its inlet is located in same water depth $D = 6.375m$. The envelop shape of the embedded single channels are presented in Fig. 4.8 and the dash line means centerline of the embedded channels. The analysis are performed in various incident wave periods $T_w/T_{ch} = 0.5 \sim 2.0$ and porosities of slit plate $r = 0.1 \sim 0.6$.

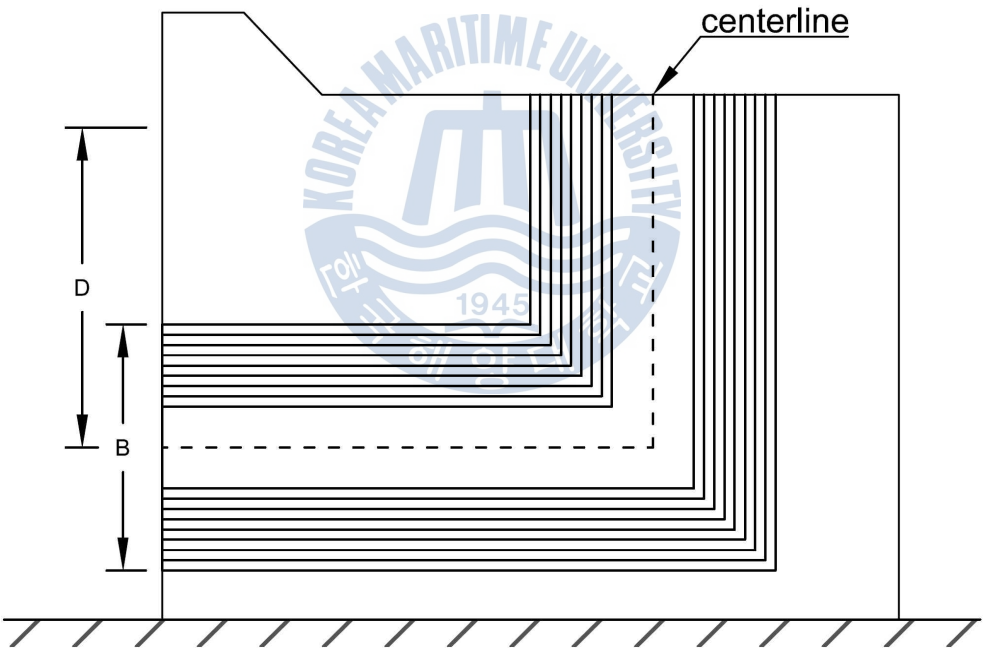

Fig. 4.8 Envelop shape of the embedded single channels $B/L_c = 0.1 \sim 0.3$ in a slit caisson breakwater

For the evaluating reflection characteristics of a slit caisson breakwater with an embedded resonant channel, the contour plots of reflection coefficients are presented as porosity r and normalized wave period T_w/T_{ch} in Fig. 4.9 and 4.10. In this figures, the reflection coefficients are shown for the various width of the embedded channels B. When the width of channel is increased, the reflection coefficients shows the two trends. One is the expansion of reflection reduced band of periods at wide width of embedded channel, and the other is that band of optimum porosities ($K_R < 20\%$) are moved to large porosity at the narrow embedded channel.

(a) $B/L_c = 0.1$

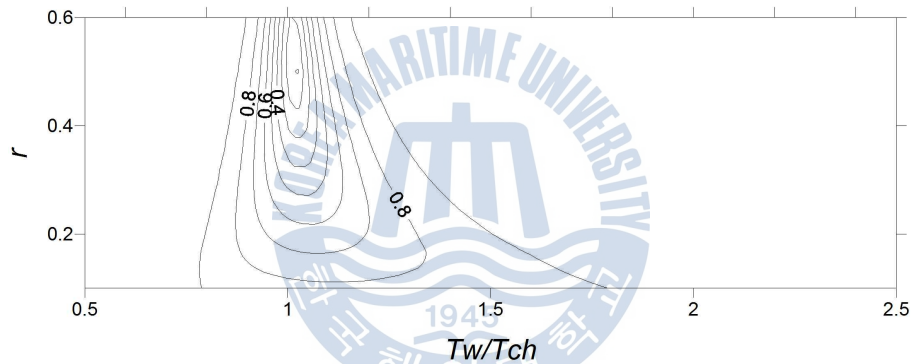

(b) $B/L_c = 0.15$

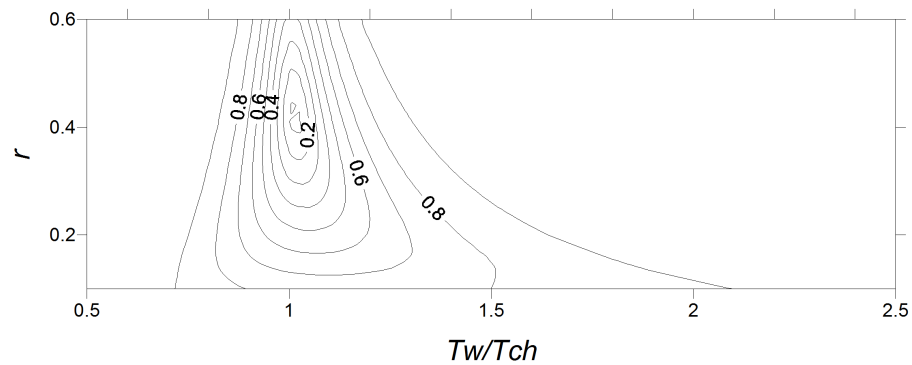

Fig. 4.9 Contour plot for reflection coefficient K_R of slit caisson breakwater with an embedded single channel $B = 0.1 \sim 0.3$ w.r.t. r and T_w/T_{ch} (1)

(c) $B/L_c = 0.20$

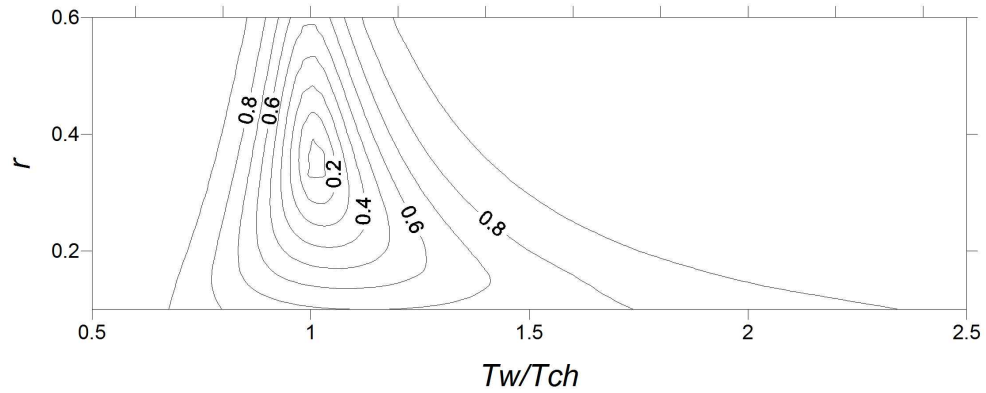

(d) $B/L_c = 0.25$

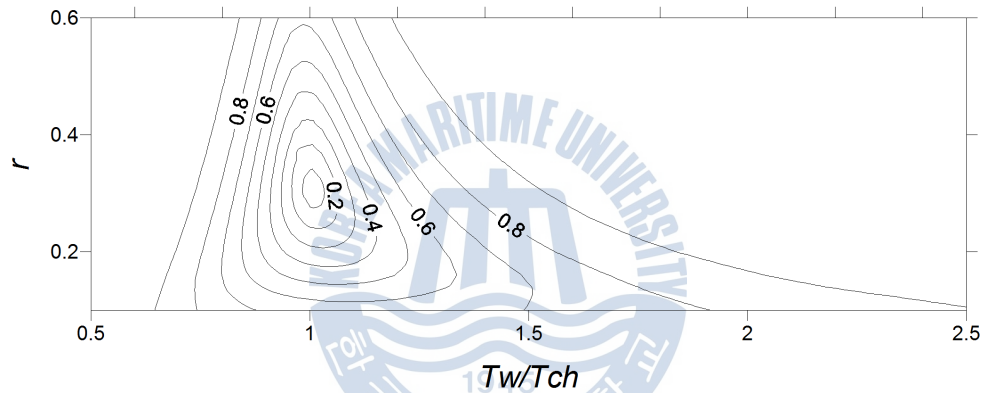

(e) $B/L_c = 0.30$

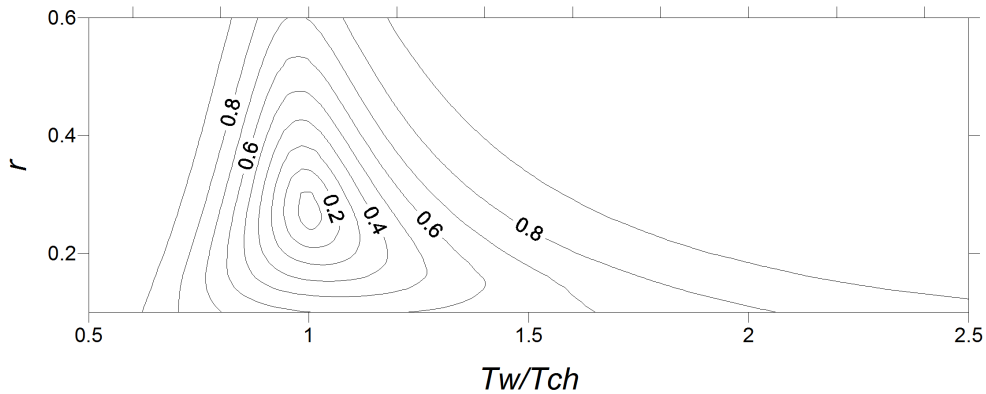

Fig. 4.10 Contour plot for reflection coefficient K_R of slit caisson breakwater with an embedded single channel $B = 0.1 \sim 0.3$ w.r.t. r and T_w/T_{ch} (2)

At the each porosities $r = 0.1 \sim 0.6$, the contour plots of reflection coefficient are presented as normalized wave period T_w / T_{ch} and normalized width of the embedded channel B/L_c for the evaluating the influence of embedded channel width in Fig. 4.11. These contours are obviously defined that the relation between the channel width and the porosity of slit plate is inverse relation as proper design condition for energy dissipation (narrow channel $B/L_c = 0.1$ and large porosity $r = 0.6$; wide channel $B/L_c = 0.3$ and low porosity $r = 0.2$). Also the width of the channel has an effect on the bandwidth of wave periods reducing reflection coefficients. The wide width of the embedded channel has an trend curves of decreased reflection coefficient at broad bandwidth of wave periods. However, the influence of channel width also has the optimum design range related with channel width B and porosity r.

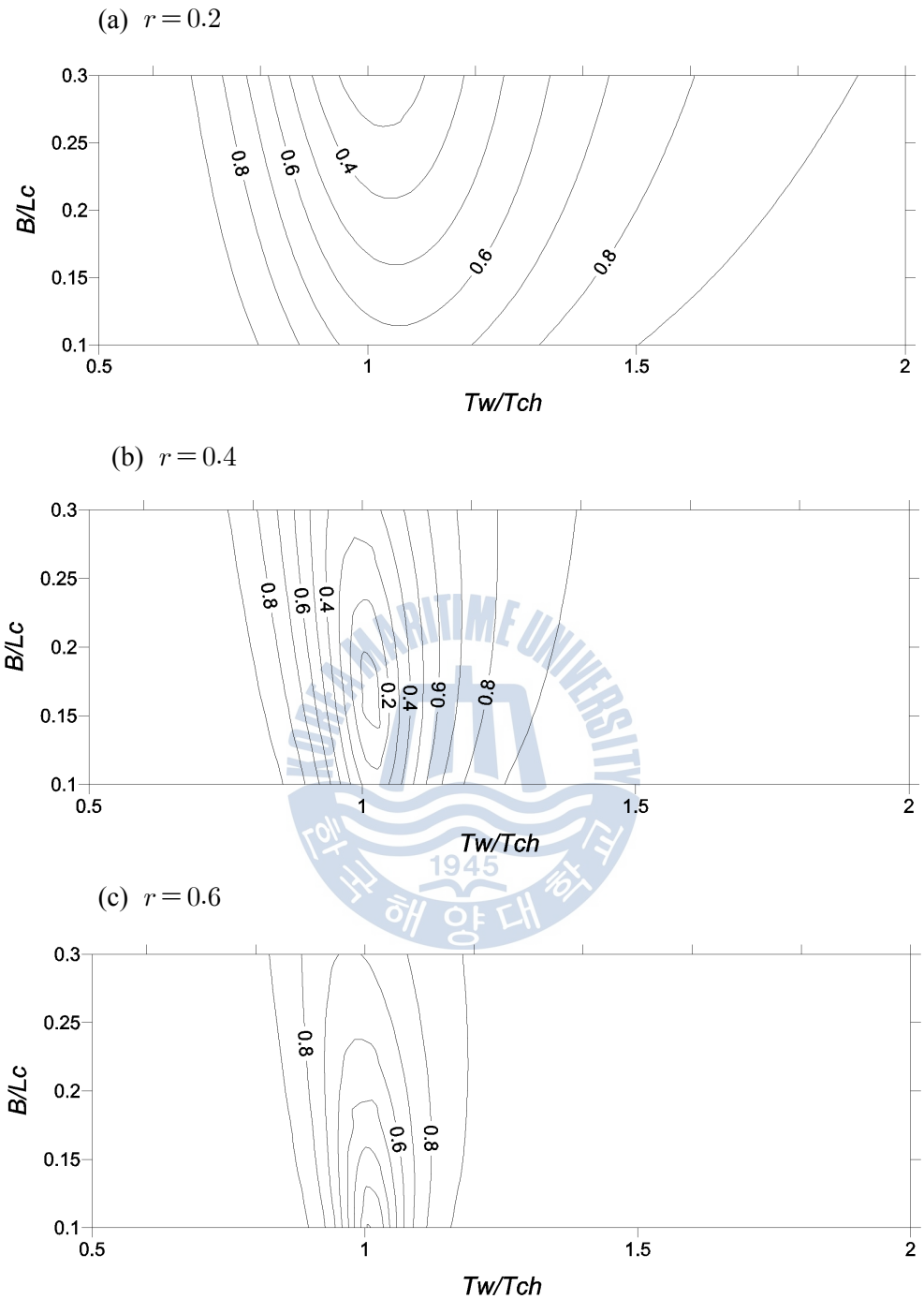

Fig. 4.11 Contour plot for reflection coefficient K_R of slit caisson breakwater with an embedded single channel $r = 0.2 \sim 0.6$ w.r.t. B/L_c and T_w/T_{ch}

The minimum reflection coefficient $K_{R_{\min}}$ is presented as porosity r and normalized width of the embedded channel B/L_c in Fig. 4.12. The tends of minimum reflection coefficient are similarly appeared inverse curve with respect to the porosity and normalized width of channel axes plane. The normalized incident wave periods T_w/T_{ch} at minimum reflection coefficient is presented in Fig. 4.13. It means that the flow of fluid in to the channel is properly formed by resonant mode of fluid in the embedded channel, so it called resonant period. The resonant periods are influenced by porosity and width of channel. At the low porosity $r=0.1$, the influence of channel width on resonant period is small and entire region is appeared the resonant period is larger than natural period of fluid in a embedded channel $T_w/T_{ch} \simeq 1.09$. When the porosity is increased, the resonant period is going to near natural period of fluid in embedded channel.

In order to know aforementioned trends of optimum porosities effected by width of the embedded channels, optimum porosities ($K_R=0.2$) are shown with respect to various width of the embedded channels $B/L_c=0.1\sim0.3$ in Fig. 4.14. When the width of the embedded channel is increasing, the optimum porosities are moved to low porosity in the entire region. In the Fig. 4.14, the upper and lower limit of optimum porosities are presented by symbol (upper limit:○, lower limit:△). And the solid line is represented as the trend line of each limits.

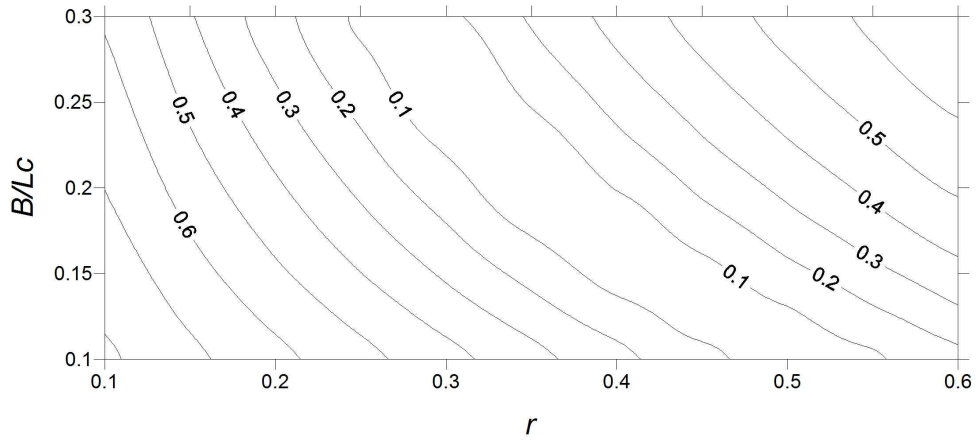

Fig. 4.12 Contour plot for minimum reflection coefficient $K_{R_{\min}}$ of a slit caisson breakwater with an embedded single channel $B=0.1\sim0.3$ w.r.t. B/L_c and r

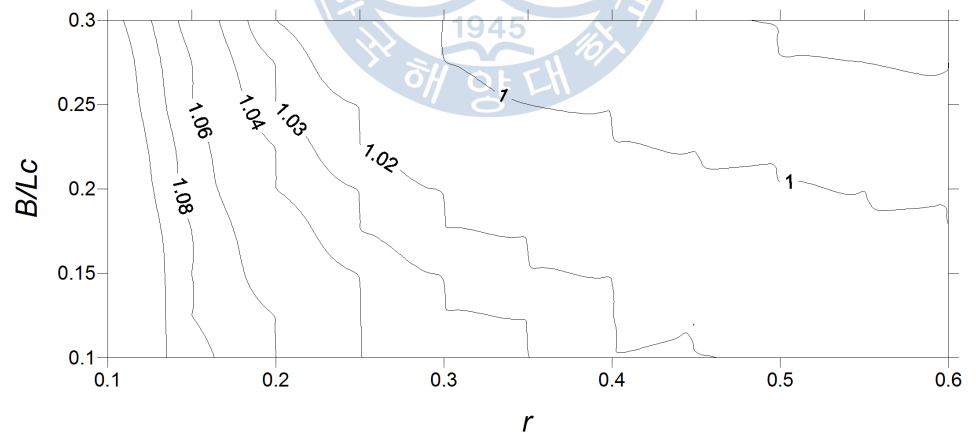

Fig. 4.13 Contour plot for normalized resonant period of a slit caisson breakwater with an embedded single channel $B=0.1\sim0.3$ w.r.t. B/L_c and r

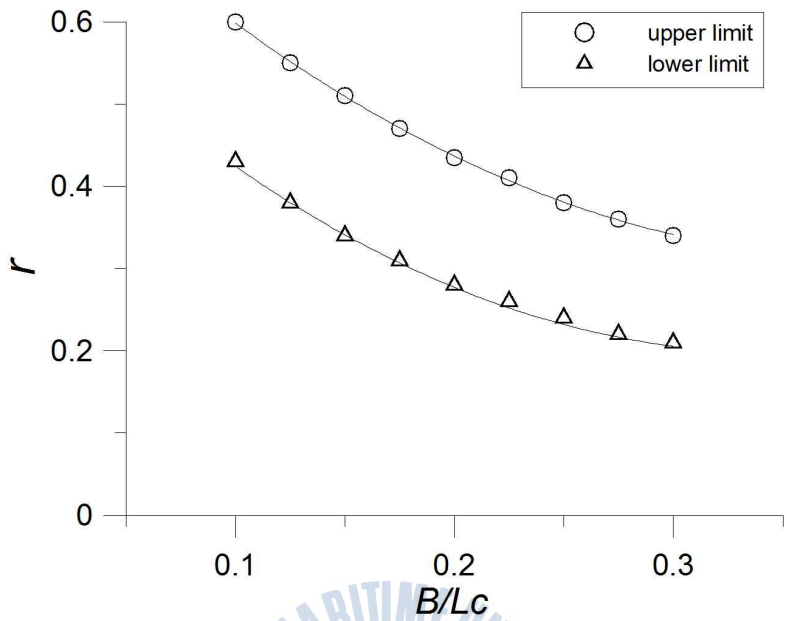

Fig. 4.14 Optimum porosity range ($K_R < 0.2$) of a slit caisson breakwater with the embedded single channel $B = 0.1 \sim 0.3$ w.r.t. B/L_c and r

In the same way, the range of porosity at various width of the embedded channel is presented as the trend lines of reflection coefficient in Fig. 4.15(a). Each of the solid lines and dash lines are trend line of upper and lower limits of target reflection coefficients(K_R=0.1~0.4). This figure will be used to determine the design parameters (r and B) of the embedded channel according to the target reflection coefficient. Also depending on the variable width of the embedded channel, incident wave period band at the target reflection coefficient K_R=0.1~0.4 are shown in Fig. 4.15(b). It is appeared that the wide width of the channel cases shows the broad bandwidth of the wave periods for target reflection coefficients.

(a) design parameters (r and B/L_c)

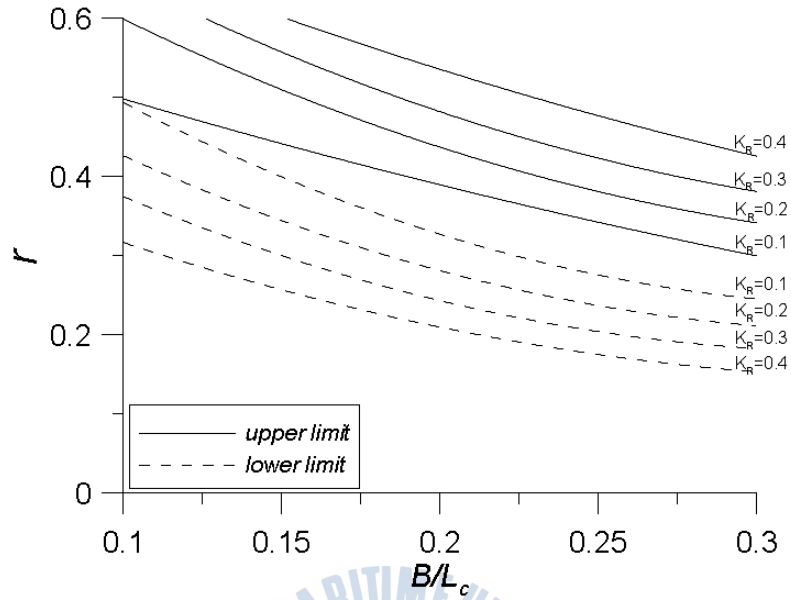

(b) wave period band (T_w/T_{ch} and B/L_c)

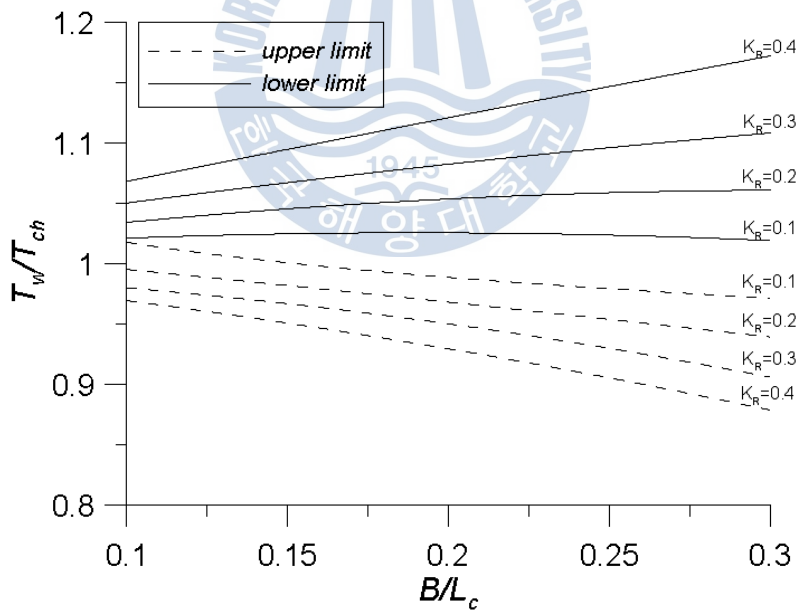

Fig. 4.15 Design parameters (r, B/L_c) and wave period band (T_w/T_{ch}) according to the target reflection coefficient (target $K_R = 0.1 \sim 0.4$)

To deal with highly irregular environment of the ocean, the various incident wave periods are considered to evaluation of reduced reflections. For evaluation of energy dissipation function of the slit caisson breakwater in target incident wave periods, the band of incident wave periods is decided considering in wave characteristics in target field. So, the evaluation is performed as the average and significant reflection coefficient. First, the evaluation is performed by the average reflection coefficient $K_{R_{ave}}$ at various band of incident wave periods. The band of incident wave periods are considered to three section $T_w/T_{ch} = 0.5 \sim 1.5,\ 0.7 \sim 1.3$ and $0.9 \sim 1.1$. The reflection coefficients are appeared to similar trends of reduced condition in Fig. 4.16. However, the reflection coefficients are shows obviously different value depending on the considered band of wave periods. Also the narrower band of incident wave period is shows the largely decreased reflection coefficients.

In the Fig. 4.15, the design parameters according to the target reflection coefficients was proposed as guide line for design of the embedded single channel. Futhermore, the application of the multi-channels was more improved the function of energy dissipation than the single channel, it was contributed to expand the design range (porosity r and target wave period T_w) representing the proper effect.

(a) $T_w/T_{ch} = 0.5 \sim 1.5$ (bandwidth of $T_w/T_{ch} = 1$)

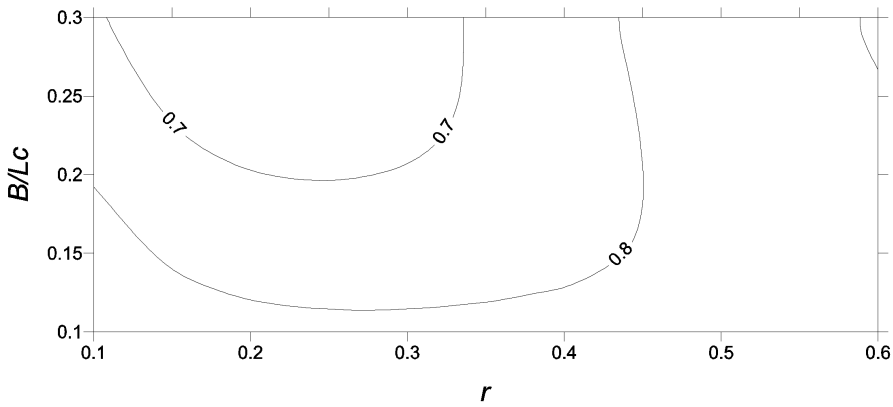

(b) $T_w/T_{ch} = 0.7 \sim 1.3$ (bandwidth of $T_w/T_{ch} = 0.6$)

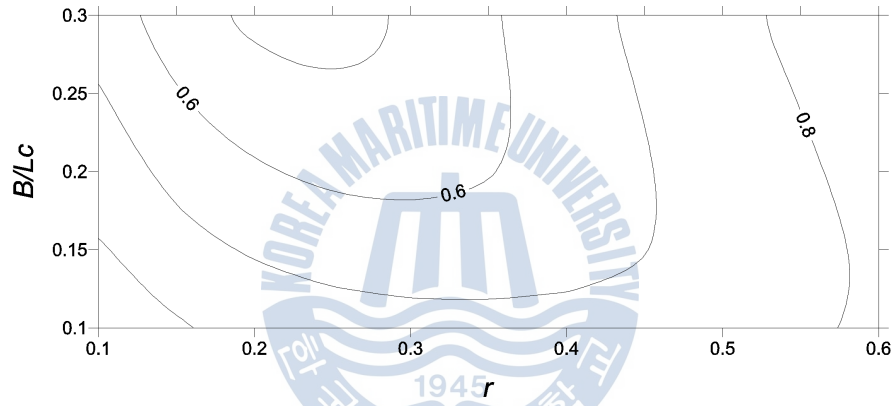

(c) $T_w/T_{ch} = 0.9 \sim 1.1$ (bandwidth of $T_w/T_{ch} = 0.2$)

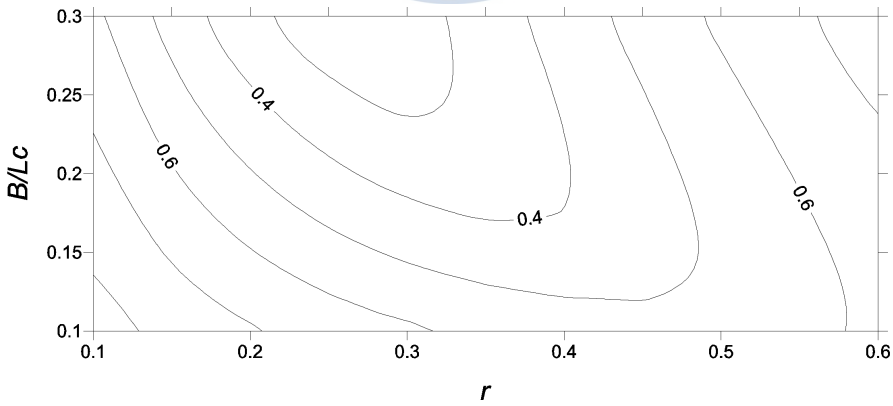

Fig. 4.16 Contour plot for the average reflection coefficient $K_{R_{ave}}$ of a slit caisson breakwater with an embedded single channel w.r.t. B/L_c and r

The other way to deal with irregular environment of the ocean is using significant reflection coefficient. In this analysis, the significant reflection coefficient is the lowest one-third of reflection coefficient. This is simply defined as the average of the lowest reflection coefficients. The trend of significant reflection coefficients are similarly appeared to the average of reflection coefficients, but the reduced amount of significant value is more smaller than average value.

For design of the slit caisson breakwater with an embedded resonant channel, the proper evaluation is essential as relationship between porosity and width of the embedded channel. Also, this relationships are to be evaluated against significant reflection coefficient and average reflection coefficient in the target band of wave periods. Furthermore, the target band of wave periods is properly determined to considering wave condition at installation sea area.

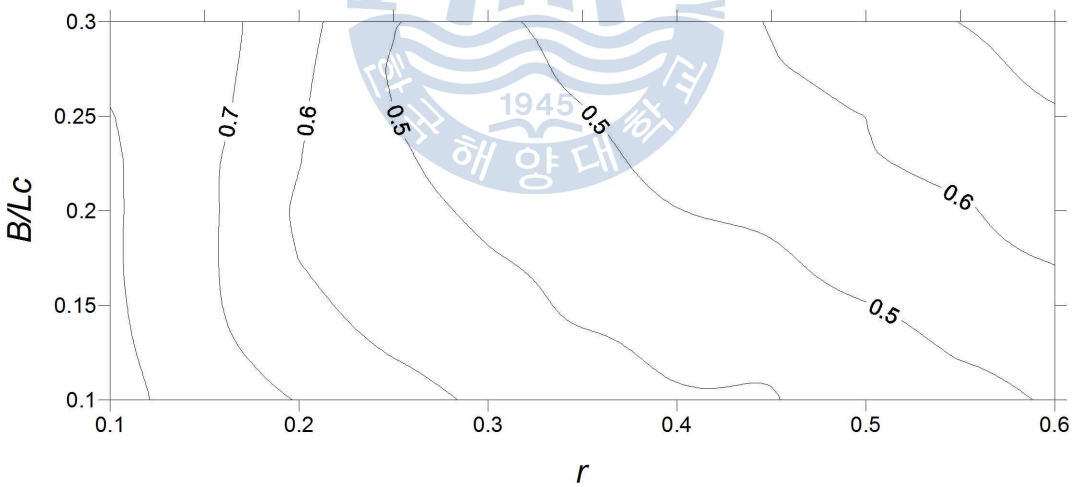

Fig. 4.17 Contour plot for the significant reflection coefficient $K_{R_{sig}}$ of a slit caisson breakwater with an embedded single channel w.r.t. B/L_c and r

4.3 Embedded Multi-Channels Case

In order to investigate the effect of multiple channels on the reflection coefficient, the analysis is performed on a slit caisson breakwater with the embedded multi-channels. In this multi-channel cases, the double and triple channels are considered. Those cases are compared with the single channel having a same width of multi-channels.

4.3.1 Comparison of double and single embedded channel

A slit caisson breakwater having the double or single embedded channels are shown in Fig. 4.18. The shape of channels in the slit caisson breakwater are represented by solid line for single channel and dash line for double channels. Each of the double channels are named for A (upper channel) and B (lower channel). The shape parameters of each channels are presented in Table 4.4 for the depth of inlet D, the width of channel B, the length of channel L_c and the natural period of channel T_n. The natural period of each channels are different, so the reacting incident wave period are different. The double embedded channel shows two resonant period caused by water column in two channels.

Table 4.4 Shape parameters of the single and double channels

Channel	D [m]	B [m]	L_c [m]	T_n [sec]
Single	6.375	4.125	16.125	8.053
Double (A)	5.0625	1.875	13.875	7.472
Double (B)	7.3215	1.875	18.375	8.599

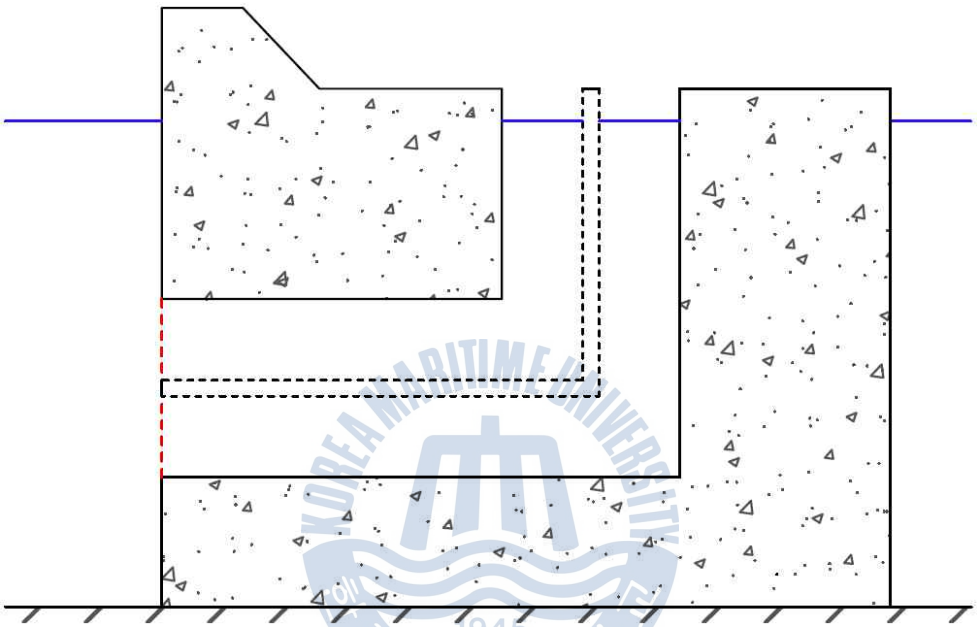

Fig. 4.18 A conceptual slit caisson breakwater with the single and double embedded channel

The element meshes for fluid region are shown in Fig. 4.19 for a slit caisson breakwaters with a embedded single channel and the embedded double channels. The 8-noded iso-parametric element is used for discretizing the entire inner fluid region, and far field region is discretized by infinite element. The meshes are consisted by finite elements and infinite elements. It is used for discretizing the fluid region. Minimum number of element for discretizing the fluid region per a wave length is 13 for horizontal direction, which is enough for interpolation of wave potential behaviors. In general, a minimum requirement is 4 for quadratic elements. The mesh conditions of each cases are presented in Table 4.5.

Table 4.5 Mesh conditions of a slit caisson breakwater with the embedded single and double channel cases

Channel	Single	Double
No. of Finite Elements	676	510
No. of Infinite Elements	21	18
No. of nodes	2209	1698

(a) single channel

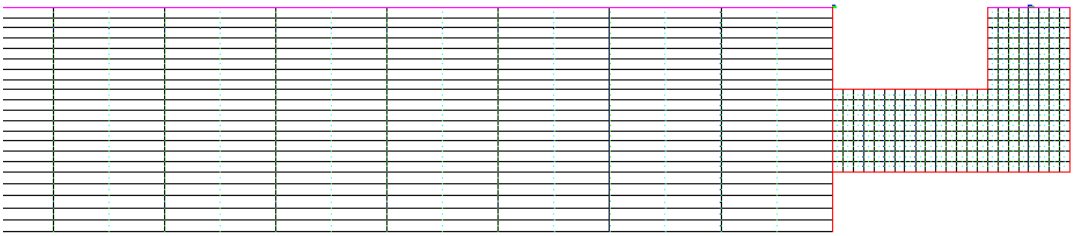

(b) double channel

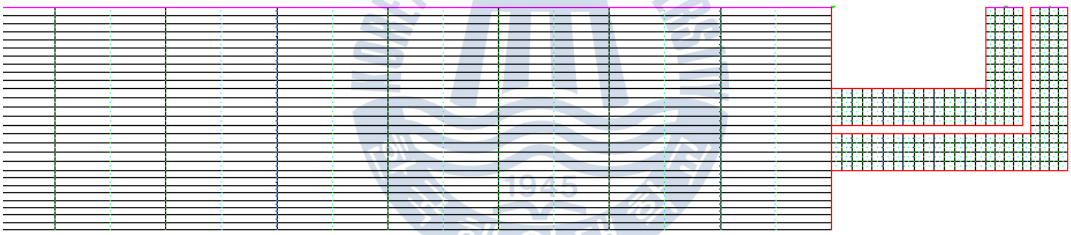

Fig. 4.19 Finite element meshes of a slit caisson breakwaters with the embedded single and double channels

In order to compare the reflection characteristics of embedded single channel and double channels, reflection coefficient is represented for normalized wave period T_w/T_{ch} and porosity r in Fig. 4.20. The porosity r is considered from 0.1 to 0.6. The reflection coefficient is affected by the porosity of slit plate. The decrease of reflection coefficient is concentrated to near natural period, especially higher porosity and it is spreaded along the various periods at lower porosity. Near the resonant period $T_w/T_{ch} \simeq 1$ in double embedded channel case, the minimum reflection coefficient shows double peaks. It is seemed that the resonant mode is properly formed at each of channels. Both cases have the similar trends of reflection coefficient except double peak. However, the porosity of the resonant mode is shifted to high porosity at double channel case because of each narrow channel width.

The minimum reflection coefficient of embedded single and double channel cases are compared in Fig. 4.21(a) and it means maximum energy dissipation at each porosity. The minimum reflection coefficients are effected by porosity. Also the lowest minimum reflection coefficients of single and double channel cases are almost zero and they are appeared at different porosities $r = 0.35$ (single channel) and $r = 0.50$ (double channels).

The periods of minimum reflection coefficients are shown in Fig. 4.21(b). The resonant periods shows similar trends between single and double channel case. When the porosity is increase, the natural period of fluid in the channel is move to longer period than natural period of the channel. Also the natural period of the double channel case has shifted to longer period than the single channel case.

(a) single channel $(B=4.125m)$ (b) double channel $(B=1.875m\times 2)$

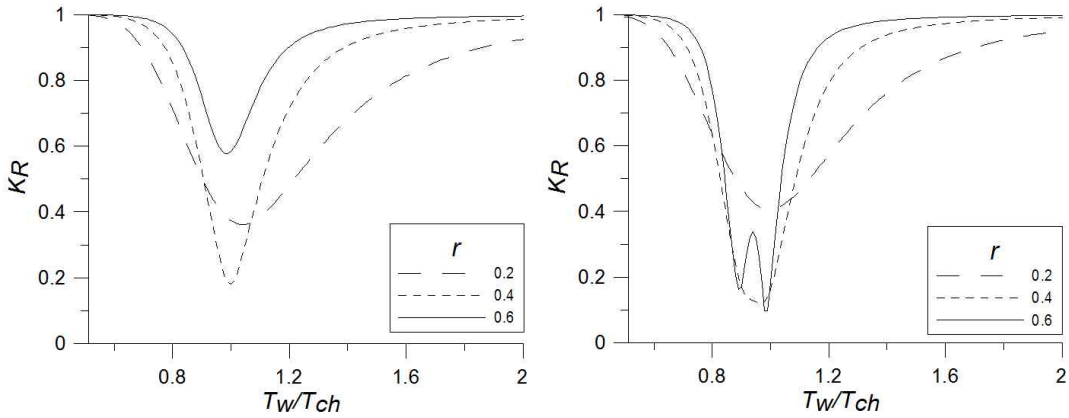

Fig. 4.20 Reflection coefficient K_R of a slit caisson breakwater with the embedded single channel and double channels

(a) $K_{R_{\min}}$ (b) T_w/T_{ch} (at $K_{R_{\min}}$)

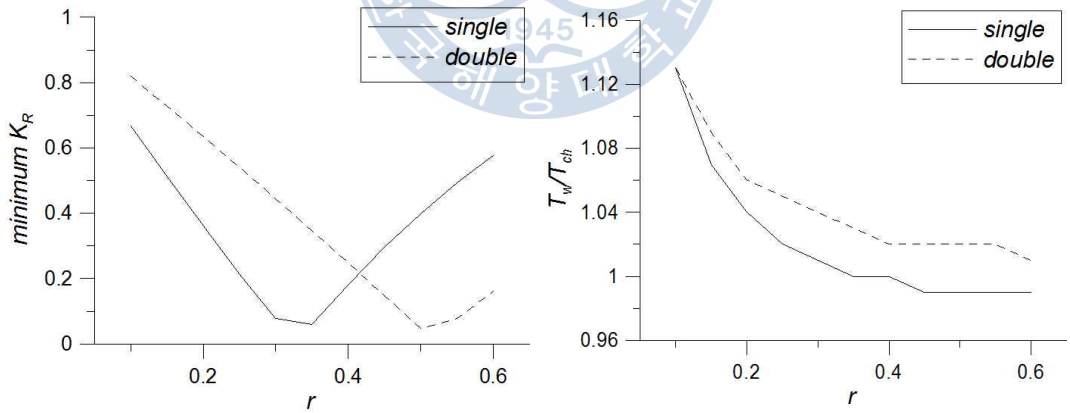

Fig. 4.21 Minimum reflection coefficient $K_{R_{\min}}$ and normalized wave period of resonant mode T_w/T_{ch} of a slit caisson breakwater with the embedded single and double channels

In order to investigate these trends of reflection coefficient affected by the porosity and wave period, the contour plot of reflection coefficient is presented as a function of normalized wave period and porosity for a slit caisson breakwater with embedded single and double channel in Fig. 4.22. In these figure, the contrast area indicates the natural periods band of the each embedded channels from the channel length. Each of cases are shown properly reduced reflection coefficient ($K_R < 0.2$) under different porosity condition and incident wave periods. Also the area of minimum reflection coefficient of the double channel case is much wider than the single channel case. The double embedded channels separates the natural periods to shorter (A channel) and longer periods (B channel). From this reason, the group of the embedded double channels affect to expanding the incident wave periods band of properly reduced reflections.

The optimum porosity of embedded single channel case is represented at $r = 0.35$, also reduction of reflection coefficient is spread on the plane region of porosity and normalized wave period. At the double embedded channels, the reduced area of reflection coefficient is larger than the single embedded channel case and the optimum porosity is expanded to $r = 0.3 \sim 0.6$.

So, the separating the embedded channels expand the optimum design conditions of properly reducing reflected waves in which optimum conditions are consisted by the porosities and incident wave periods.

(a) single channel $(B=4.125m)$

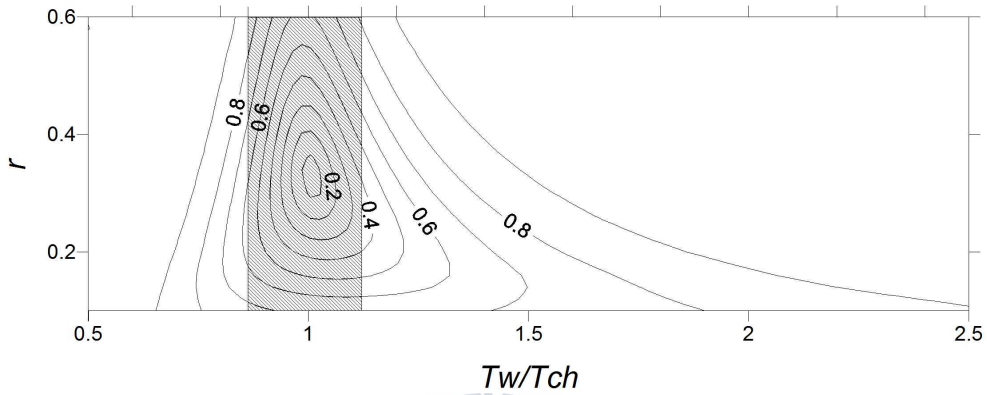

(b) double channel $(B=1.875m\times 2)$

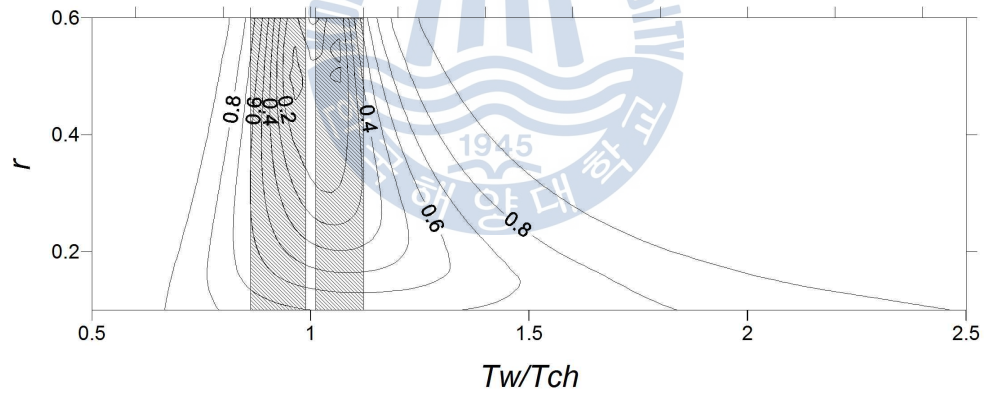

Fig. 4.22 Contour plot for reflection coefficient K_R of a slit caisson breakwater with the embedded single and double channels w.r.t. r and T_w/T_{ch}

4.3.2 Comparison of triple and single embedded channel

For comparison of the triple with single channel cases, the model is set in Fig. 4.23. The channel shape is shown solid line for single channel and dash line for triple channels. The triple channels are named for A, B and C, from top to bottom. The shape parameters of the each channels are represented in Table 4.6 for the depth of inlet D, the width of channel B, the length of channel L_c and the natural period of channel T_n.

Table 4.6 Shape parameters of the single and triple channels

Channel	D [m]	B [m]	L_c [m]	T_n [sec]
Single	5.0625	6.375	18.375	8.599
Triple (A)	5.0625	1.875	13.875	7.472
Triple (B)	7.3215	1.875	18.375	8.599
Triple (C)	9.5625	1.875	22.875	9.595

The element meshes for fluid region are shown in Fig. 4.24 for a slit caisson breakwater with embedded single channel and embedded triple channel. The 8-noded iso-parametric element is used for discretizing the channel region and the inner fluid region. The far field region is discretized by infinite element. Minimum number of element for discretizing the fluid region per a wave length is 14 for horizontal direction, which is enough for interpolation of wave potential behaviors. The mesh conditions of each cases are presented in Table 4.7.

Table 4.7 Mesh conditions of a slit caisson breakwater with the embedded single and triple channel cases

Channel	Single	Triple
No. of Finite Elements	780	742
No. of Infinite Elements	21	20
No. of nodes	2527	2540

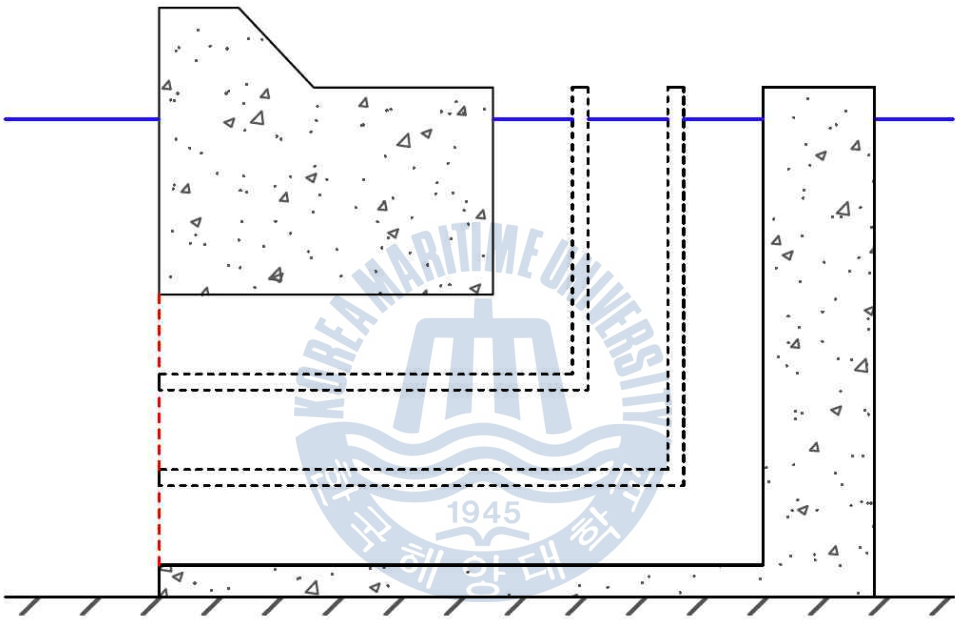

Fig. 4.23 A conceptual slit caisson breakwater with the embedded single and triple channels

(a) single channel

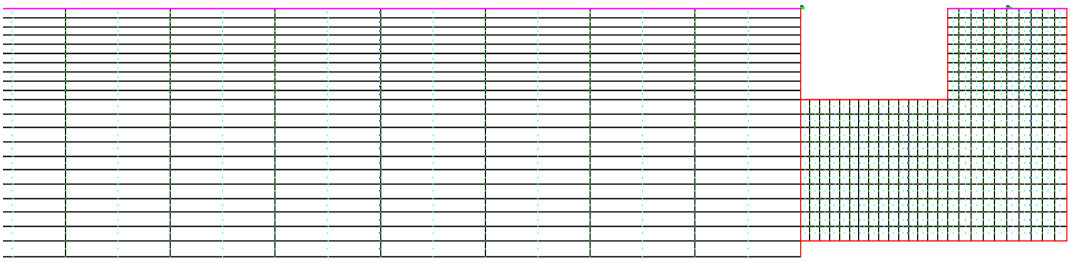

(b) triple channel

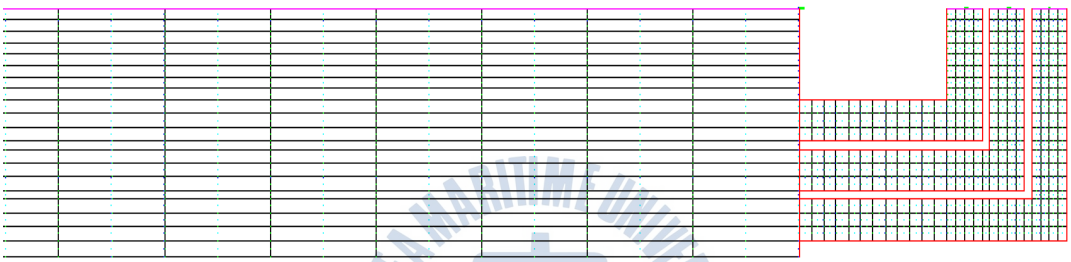

Fig. 4.24 Finite element meshes of a slit caisson breakwater with the embedded single and triple channel

In order to investigate the effects of the porosity and three channels to reflection coefficient, contour plot of reflection coefficients are presented as a function of normalized wave periods and porosities. In this analysis, the wave height is applied to $H = 0.75m$ and the porosities are considered from 0.1 to 0.6. The wave period is considered to near natural period of an embedded single channel $T_w / T_{ch} = 1$ and the range of incident wave periods are $T_w / T_{ch} = 0.5 \sim 2.0$.

The reflection coefficients of the embedded single and triple channels are represented in Fig. 4.25. In this figure, the reflection coefficient trends of triple embedded channel shows three peaks at near the each natural period of channels and the wave period band of minimum reflection coefficient is expanded to wider than

single channel case at near resonant period of the channel centerline, $T_w/T_{ch}=0.85\sim1.15$ at $r=0.6$. The reflection coefficient of single channel is decreased by increasing porosity, but triple channel case shows dissimilar trend. It is suggested that the optimum energy dissipation condition is influenced by wave period with porosity of slit plate, so it is necessary to analyze together with these terms.

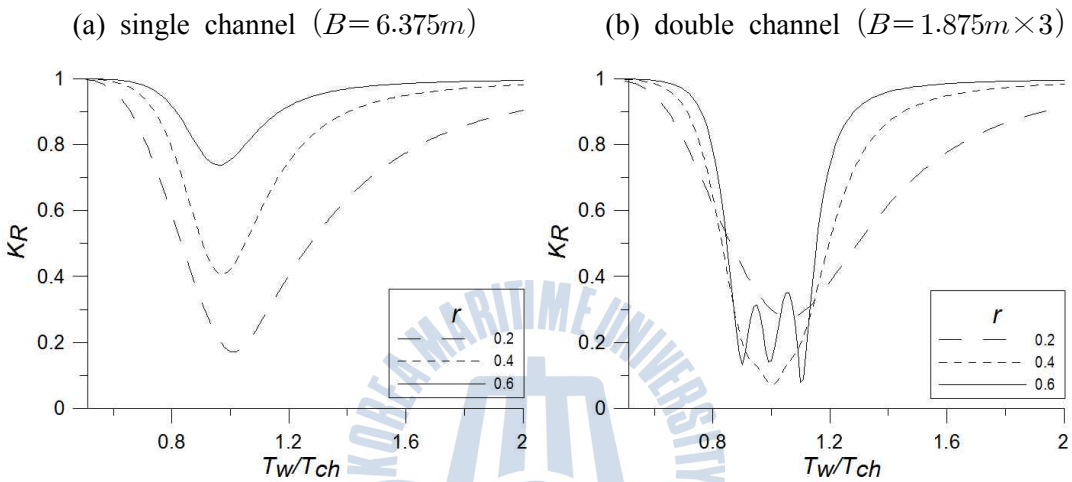

Fig. 4.25 Reflection coefficient K_R of a slit caisson breakwater with the embedded single and triple channels

For more analysis of these reflection coefficient trends effected by the porosities and incident wave periods, the contour plot of reflection coefficient is presented as a function of normalized wave period and porosity for a slit caisson breakwater with the embedded single and triple embedded channels in Fig. 4.26. In these figures, the contrast are indicates the natural periods band of the each embedded channels from the channel length. Each of cases are shown properly reduced reflection coefficients ($K_R<0.2$) under different porosity and wave periods. Also the minimum reflection coefficient area of the embedded triple channel case is much wider than the embedded single channel case. Each of three channels

separates the natural periods to shorter and longer periods. From this reason, the group of the embedded triple channels affect to expanding the incident wave periods band of properly reduced reflections.

The optimum conditions ($K_R < 0.2$) of an embedded single channel case is appeared at porosity $r = 0.25$ and normalized wave periods $T_w / T_{ch} = 0.92 \sim 1.08$. At the triple channel case, the optimum conditions are expanded to wider than single channel case, these are the porosities $r = 0.25 \sim 0.6$ and the normalized wave periods $T_w / T_{ch} = 0.88 \sim 1.12$.

So, the using the embedded multi-channels expand the range of optimum design conditions of considerable energy dissipation in which optimum conditions are consisted by the porosities and incident wave periods.

The minimum reflection coefficient according to the change of porosity is shown in Fig. 4.27(a) and it is compared single with triple embedded channel case. The each of minimum values are effected by porosity. The lowest minimum reflection coefficients are almost zero and they are appeared at different porosity $r = 0.25$ (single channel) and $r = 0.50$ (triple channel). In the triple embedded channel case, the minimum reflection coefficients formed as an flat arc curve under $K_R < 0.6$. The minimum reflection coefficient of the single channel case shows steep linear line and they are higher than triple channel case at $r > 0.3$.

The periods of minimum reflection coefficient are compared the single with triple channel case in Fig. 4.27(b). The resonant periods of the single and triple channel have similar trends in the whole porosity region except $r = 0.55 \sim 0.6$. When the porosity is increase, the natural period of fluid in the channel is move to longer period than natural period of the channel. On the other hand the resonant period of the triple channel case shows longer than single channel case except $r = 0.55$.

(a) single channel ($B=6.375m$)

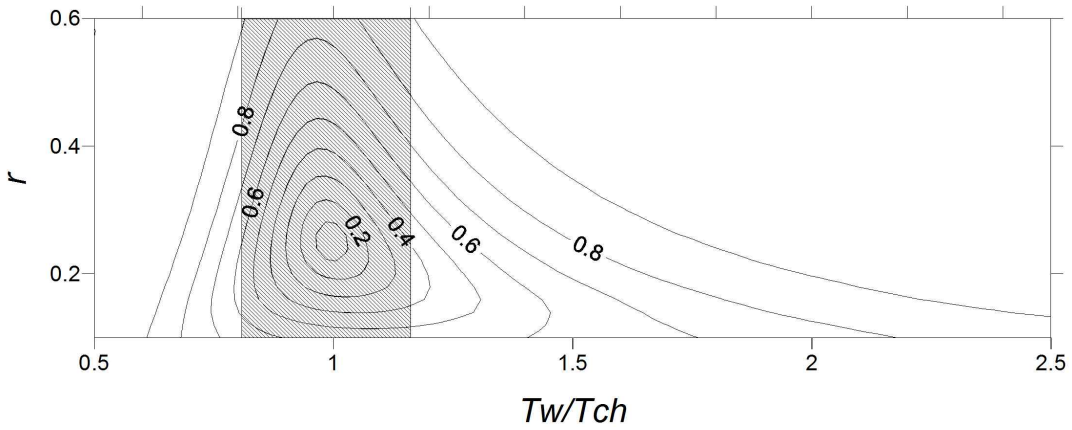

(b) triple channels ($B=1.875m\times3$)

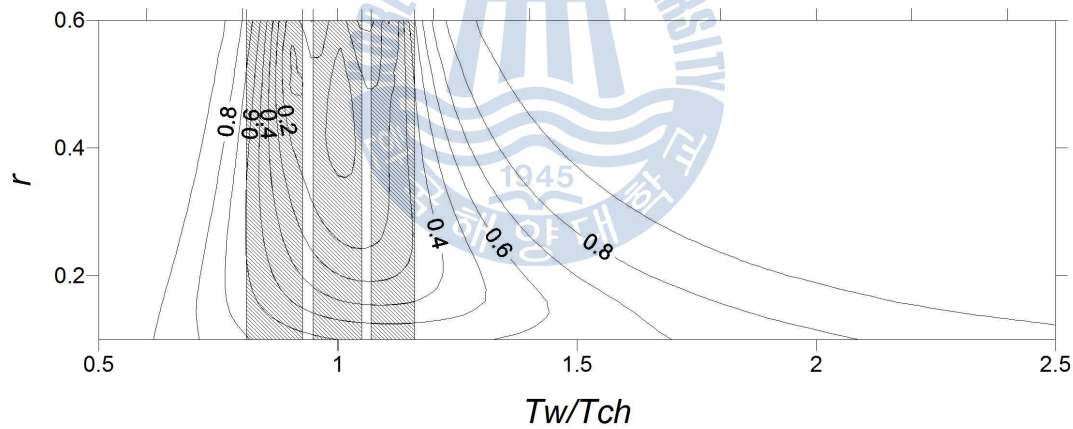

Fig. 4.26 Contour plot for reflection coefficient K_R of a slit caisson breakwater with the embedded single and double channels w.r.t. r and T_w/T_{ch}

In the Fig. 4.28, the design parameters are plotted together single (solid line) and multi-channel case. The multi-channel cases were considered double and triple embedded channels and these porosity of target reflection coefficient are plotted as the symbols. In the whole region of multi- channel cases, the upper limit of optimal porosities were satisfied all porosity region.

So, the lower limit of multi-channel (double and triple channel) is only plotted in Fig. 4.28. Also the multi-embedded channels separates the natural periods to shorter (upper channel) and longer periods (lower channel) under the reflection coefficient $K_R < 0.2$. From this reason, the incident wave period band of the multi-channel showing the considerably reduced reflection were more expanded than the single channel in Fig. 4.29, in which the embedded double channel and triple channel results are plotted at $B/L_c = 0.2$ and $B/L_c = 0.3$.

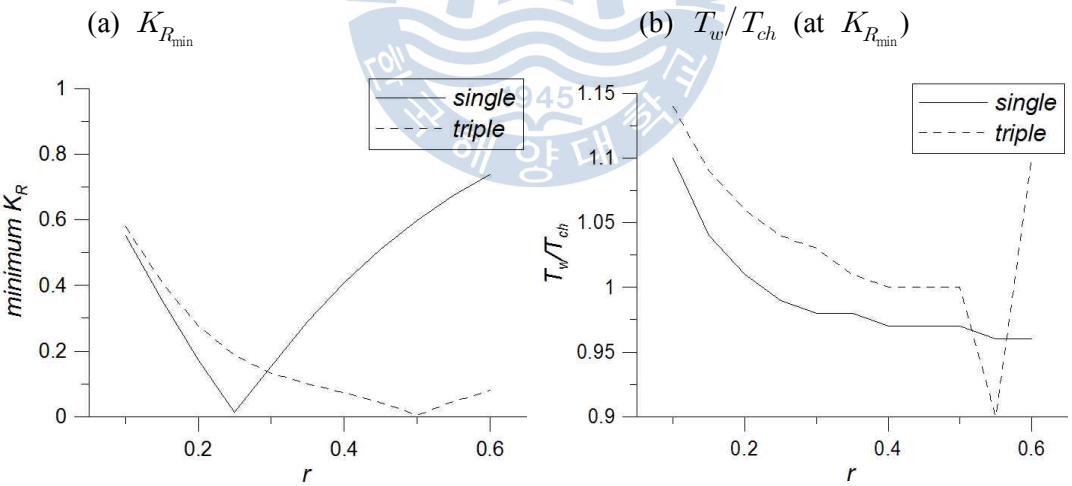

Fig. 4.27 Minimum reflection coefficient $K_{R_{\min}}$ and normalized wave period of resonant mode T_w/T_{ch} of a slit caisson breakwater with the embedded single and triple channels

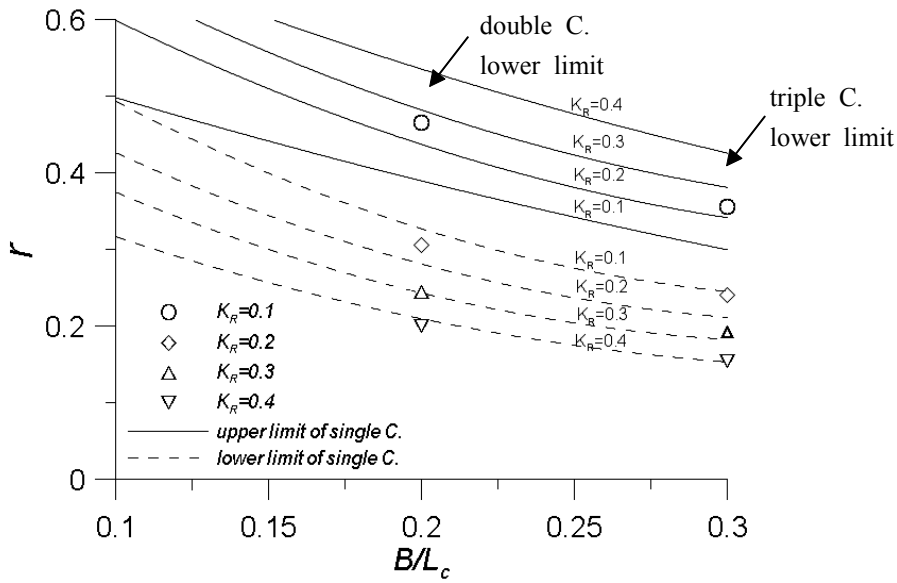

Fig. 4.28 Design parameters (r and B/L_c) of the embedded single and multi-channel according to the target reflection coefficient ($K_R = 0.1 \sim 0.4$) on numerical results

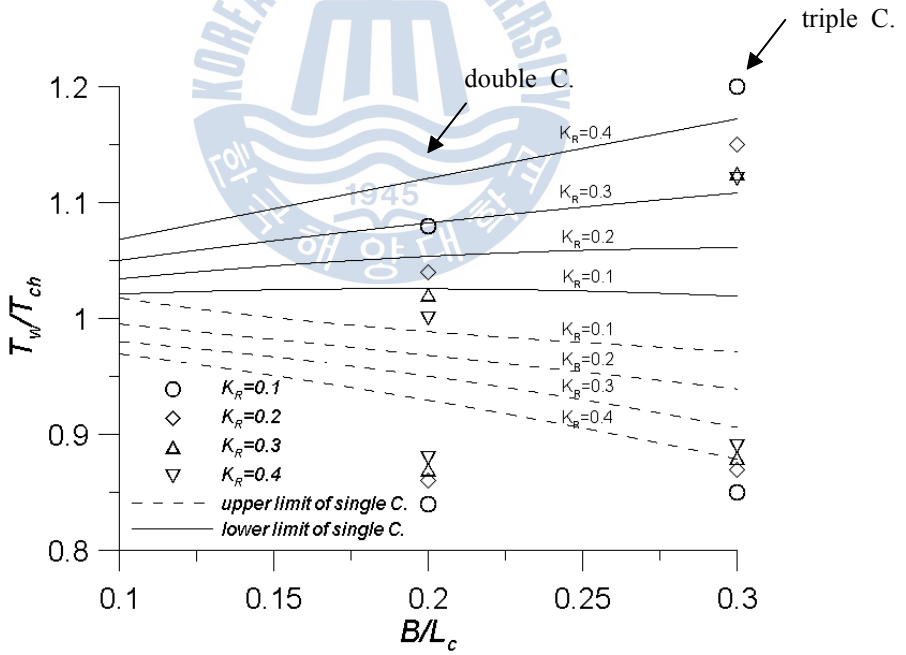

Fig. 4.29 Design parameters (T_w/T_{ch} and B/L_c) of the embedded single and multi-channel according to the target reflection coefficient ($K_R = 0.1 \sim 0.4$)

4.4 Comparison with other research

Fugazza and Natale (1992) showed that the reflection coefficient of a perforated wall caisson lying on a flat sea bottom by normalized incident wave length L and width of water chamber B between perforated-wall and caisson. The reflection coefficient is minimum at $B/L \simeq 0.25$. Water depth h=3m, water chamber width B=4m, and porosity of wall r=0.3 and 0.6 were used. For compare with present study, wave length was transformed to wave period and it was normalized with the channel natural period of present study in Figs. 4.30 and 4.31.

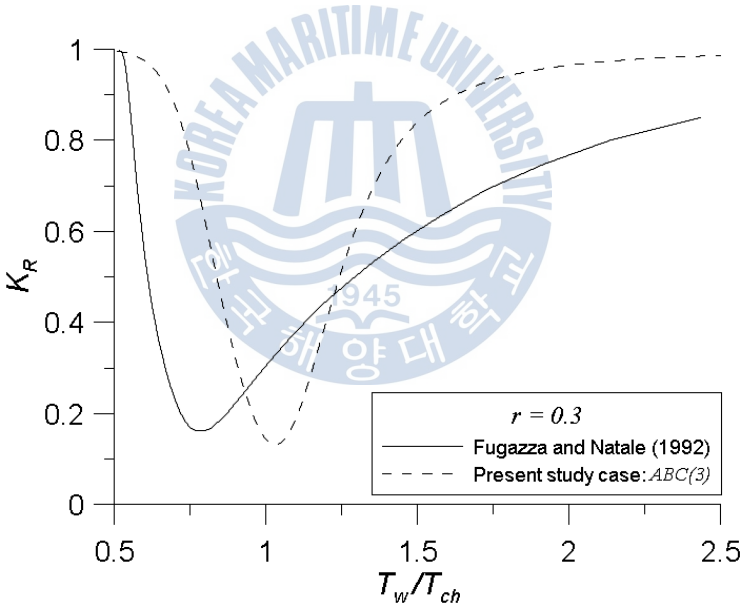

Fig. 4.30 Comparison of reflection coefficient K_R between present study and the solution of Fugazza and Natale (1992). w.r.t. T_w/T_{ch} and K_R, (r=0.3)

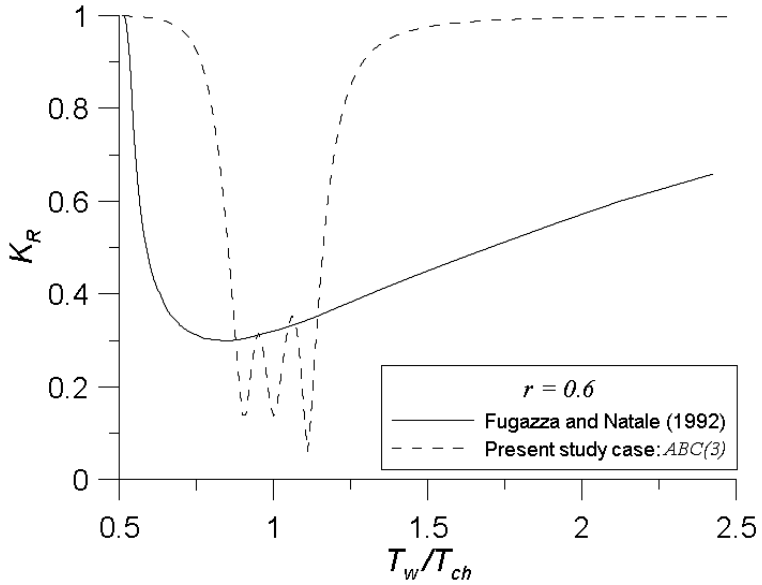

Fig. 4.31 Comparison of reflection coefficient K_R between present study and the solution of Fugazza and Natale (1992). w.r.t. T_w/T_{ch} and K_R, (r=0.6)

The reflection coefficient of porosity r=0.3 has a similar reducing trend in wave periods. In the Fig. 4.31, the reduced reflection coefficients of a perforated-wall caisson are more broadly spreaded than present study. The wave period of lowest reflection coefficient can control from design of chamber or channel. However, the size of a perforated-wall caisson model of Fugazza and Natale was B=4m and h=3m. The caisson and perforated-wall were individually consisted and the width of water chamber is relatively too wide considering water depth.

Although band of reduced reflection coefficient of present study are smaller than the traditional model, a caisson breakwater using embedded channel can be utilized by near specific target wave periods. Also, present model can protect to slit-part.

CHAPTER 5

HYDRAULIC MODEL TEST

5.1 General

To verify the present numerical results, hydraulic model experiment was carried out in the 2-dimensional wave flume at Korea Institute of Ocean Science and Technology (KIOST).

5.2 Wave Flume

The hydraulic model tests of a slit caisson breakwater with resonant channels were performed in two dimensional wave flume as shown in Fig. 5.1 and it is consisted by $53m(L)\times1m(B)\times1.25m(H)$. The piston type wave maker was installed at the upstream of wave flume and the wave absorbers were installed at the downstream of wave flume and at backside of wave maker.

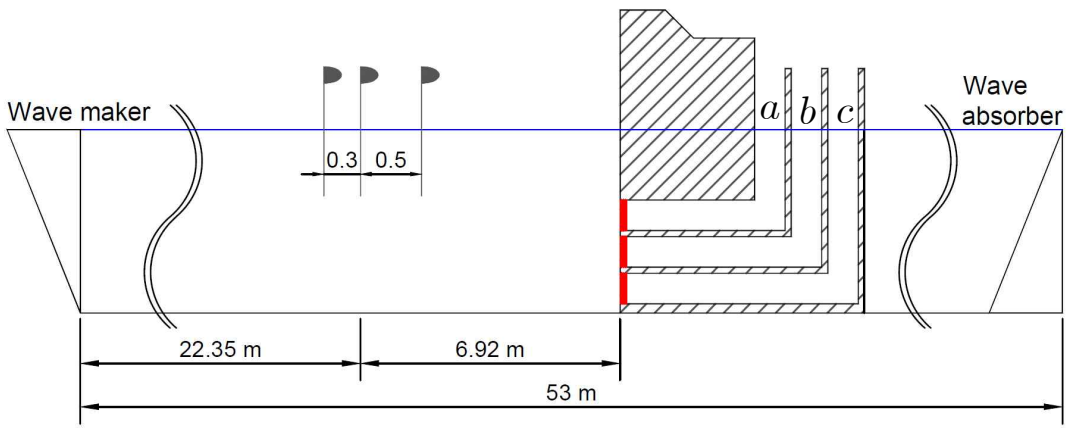

Fig. 5.1 Two dimensional wave flume and model set-up (unit: m)

5.3 Model Set-up

The model of slit caisson breakwater with resonant channels was scale downed (Froude similarity, 1:37.5) by comparing with numerical model. This model was produced by acrylic material and was fixed on the wave flume bottom. It is shown in Fig. 5.1. This model has the three channels which separated by the acrylic plates. In order to open or close the channel inlet and to change the opening ratio of the slit plates, the slit plates or the solid walls are installed at the front side of the channel inlet. The water depth of wave flume was 0.3m. The wave height was measured by the capacity type wave height meter in 25Hz.

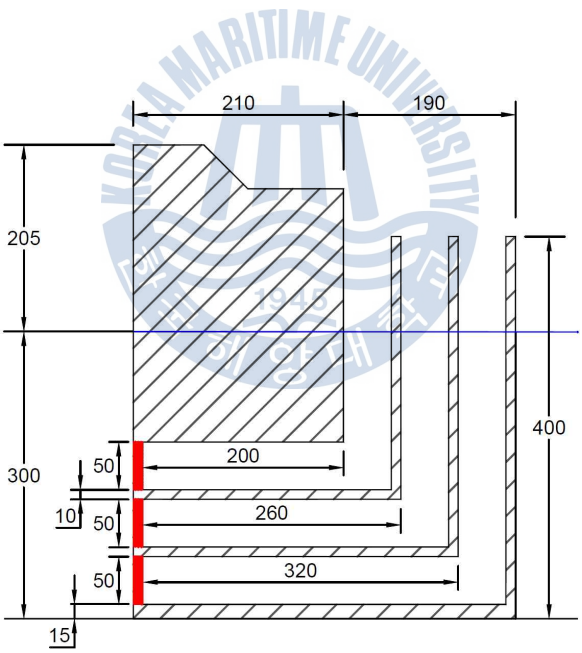

Fig. 5.2 Sectional view of a slit caisson breakwater model with resonant channels (unit: mm)

Fig. 5.3 Hydraulic model experiment set-up

This model has the three channels which separated by the acrylic plates. In order to open or close the channel inlet and to change the opening ratio of the slit plates, the slit plates or the solid walls are installed at the front side of the channel inlet. The water depth of wave flume was 0.3m. The wave height was measured by the capacity type wave height meter in 25Hz.

The channels in the caisson breakwater are named as alphabet a, b and c. The separating acrylic plates between the each channels are detachable devices for separation of the channels. The number of channels considered in the model test are from one to three. The property of the channels and hydraulic model test cases are summarized in Table 5.1. The test cases are selected for comparing with results of the numerical analysis. The regular waves are considered and wave height is 1cm. Also the wave periods and the porosity of the slit plate are follow as:

Table 5.1 Summary of hydraulic model test cases

Case ID	Number of channel	Open channel	Closed channel	Width of channel (mm)	L_{ch} (mm)	T_{ch} (s)	porosity
A	1	a	b, c	50	375	1.23	0.2 0.4 0.6
B	1	b	a, c	50	495	1.41	
$AB(1)$	1	a+b	c	110	430	1.32	
$AB(2)$	2	a	c	50	375	1.23	
		b		50	495	1.41	
$ABC(1)$	1	a+b+c	-	170	490	1.40	
$ABC(3)$	3	a	-	50	375	1.23	
		b	-	50	495	1.41	
		c	-	50	615	1.57	

The wave energy dissipation at the slit plates are influenced by porosity (opening ratio) of the slit plate. The porosities of the slit plate are considered from 0.2 to 0.6. The geometrical properties of the slit plates are shown in the Table 5.2. In the Table 5.2, r is the porosity (opening ratio) of the slit plate, α is the energy loss coefficient of the slit plate and l is the length of the jet flow. Also the C_c is the empirical contraction coefficient at the slit wall, its value was proposed by kim (1998).

Table 5.2 Geometrical properties for the slit plate and coefficients related to energy loss due to flow separation

d $[mm]$	a $[mm]$	A $[mm]$	r $\left(=\frac{a}{A}\right)$	α $\left(=\left[\frac{1}{r\,C_c}-1\right]^2\right)$	l $[mm]$	Remarks
8	2	10	0.2	37.73	47.75	$C_c=0.7$
8	5.3	13.3	0.4	6.68	20.90	
8	12	20	0.6	1.91	10.71	

(a) $r = 0.2$

(b) $r = 0.4$

(c) $r = 0.6$

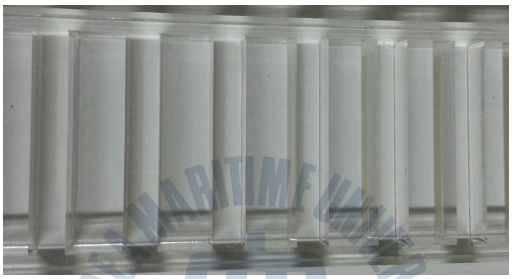

Fig. 5.4 Slit plate of hydraulic model experiment ($r = 0.2,\ 0.4,\ 0.6$)

The snapshot of hydraulic experiments is shown in Fig. 5.5. In this figure, the oscillation flow in the embedded channel is amplified from incident waves.

(a) creast

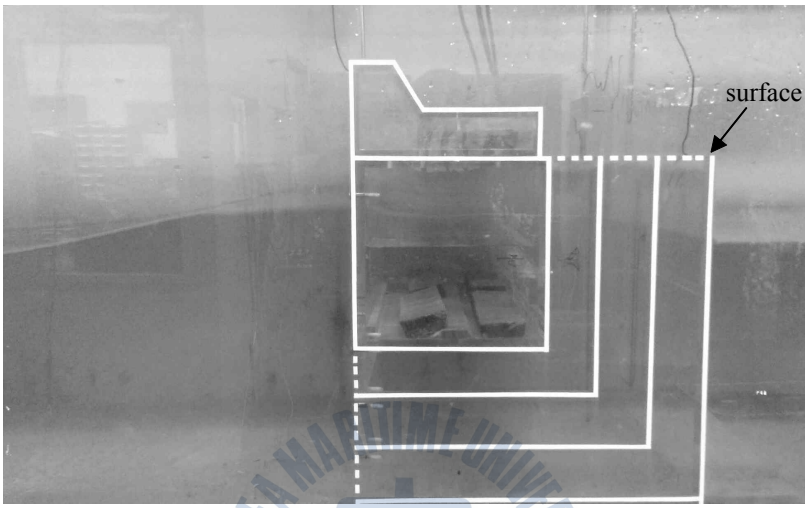

(b) trough

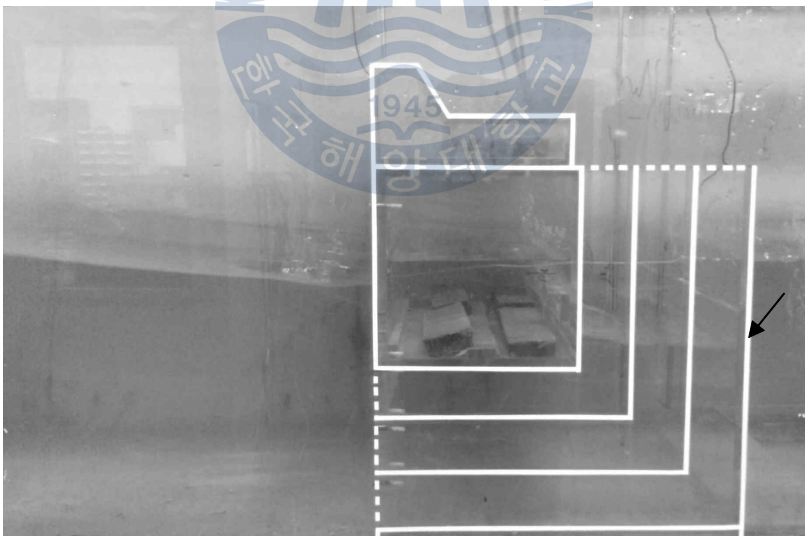

Fig. 5.5 Wave form and surface elevation in the embedded single channel (Case: $ABC(1)$, $P=0.2$, $T_w=1.67s$)

At the separated channel cases (case: $AB(2)$, $P=0.2$), fluid motion of water column in the embedded channel is differently oscillated at the each channels.

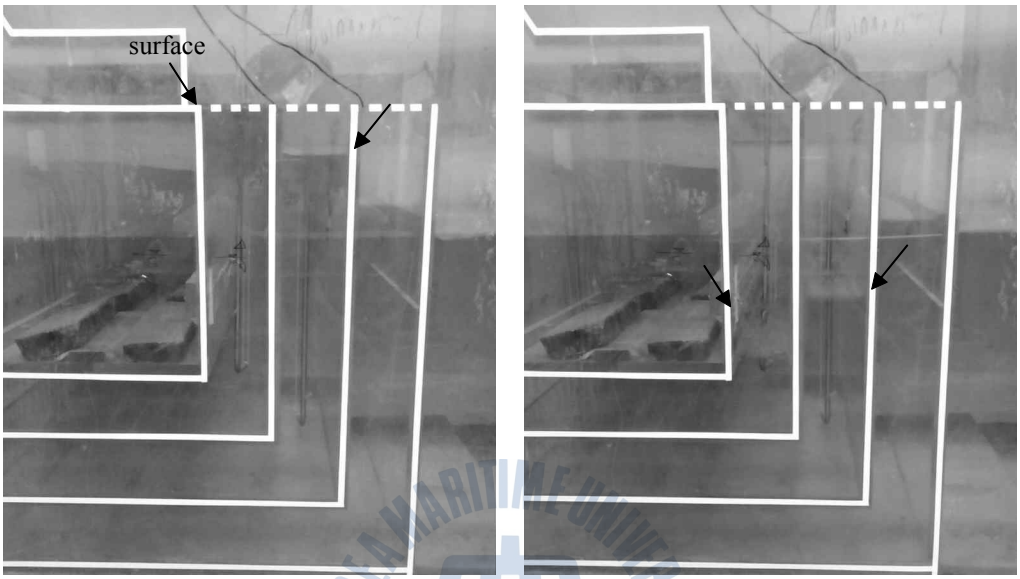

Fig. 5.6 Surface elevation in the embedded double channel
(Case: $AB(2)$, $P=0.2$, $T_w=1.67s$)

5.4 Experiment Analysis

The incident waves of the experiment is considered as regular waves, its periods T_w and normalized wave periods of each cases T_w/T_{ch} are shown in Table 5.3. These wave periods are selected at near the natural periods of the channels and the wave height H_w is 0.02m.

Table 5.3 Regular wave periods for each test conditions

Case ID / T_w (sec)	A T_{ch} =1.23 (sec)	B T_{ch} =1.41 (sec)	$AB(1)$, $AB(2)$ T_{ch} = 1.32 (sec)	$ABC(1)$, $ABC(3)$ T_{ch} = 1.40 (sec)
	T_w/T_{ch}			
1.18	0.96	0.84	0.89	0.84
1.23	1.00	0.87	0.93	0.88
1.29	1.05	0.91	0.98	0.92
1.35	1.10	0.96	1.02	0.96
1.42	1.15	1.01	1.08	1.01
1.49	1.21	1.06	1.13	1.06
1.57	1.28	1.11	1.19	1.12
1.67	1.36	1.18	1.27	1.19
1.77	1.44	1.26	1.34	1.26
1.89	1.54	1.34	1.43	1.35
2.02	1.64	1.43	1.53	1.44

5.4.1 Separation of incident and reflected waves

For separating the incident and reflected waves, the three of the wave probe were set in front of the caisson breakwater model in Fig. 5.1. The separation technique of incident and reflected waves were proposed using two wave probes (Goda and Suzuki, 1976; Goda, 1985) and using three wave probes (Mansard and Funke, 1980; Park et al., 1992). The separating incident and reflected wave using two wave probes, there are existing no solution region depending on wave

condition so that separable wave condition is limited. Also this technique is very sensitive from transverse wave in wave flume, non-linear wave interference, signal noise and measuring errors. On the other hand, the using three wave probes are less sensitive in there phenomenons. In this experimental analysis, the separation of incident and reflected waves are performed by using three wave probes and applying the least squares method (Park et al., 1992).

At three of wave probes, the measured time series data of the free surface are separated to incident and reflected waves. For example, these time series data of [case: $ABC(1),\ P=0.2,\ T_w=1.67s$] are shown in the Fig. 5.7.

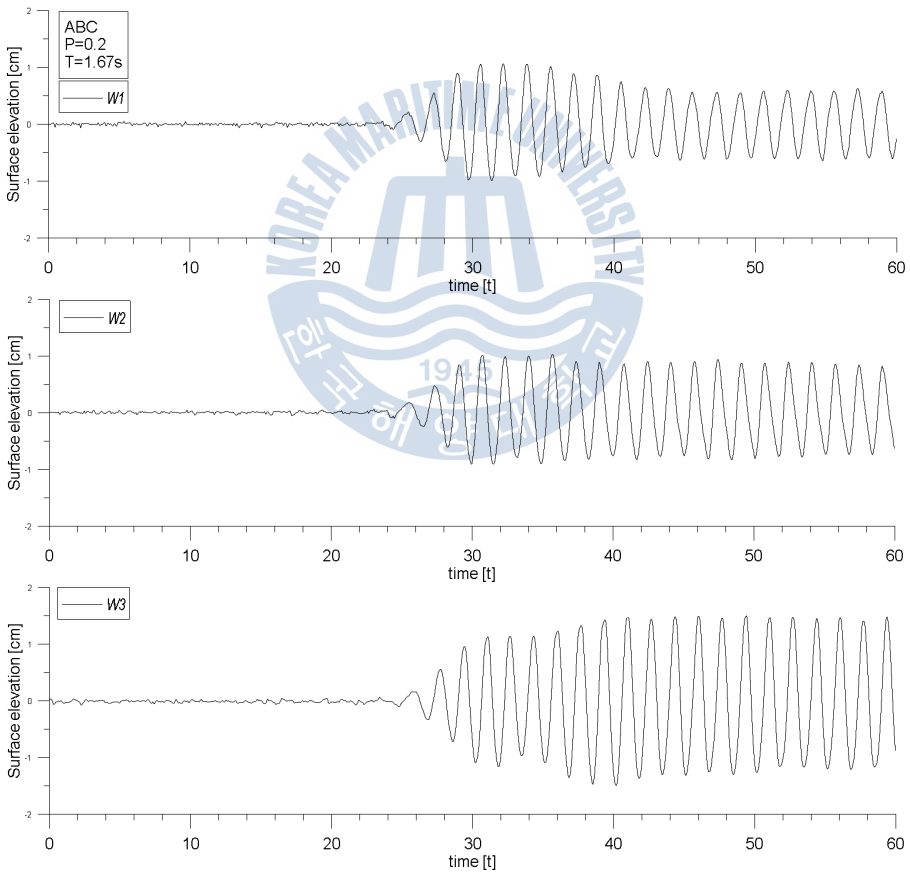

Fig. 5.7 Time series data of free surface elevation at wave probes

(Case: $ABC(1),\ P=0.2,\ T_w=1.67s$)

As results from separation of the incident and reflected waves, the reflection coefficients K_R of the experiments are shown in Figs. 5.8–5.10. The reflection coefficient of the each cases are compared by porosities between 0.2 and 0.6 and presented as normalized wave period T_w/T_{ch} in the Table 5.3.

(a) single A (b) single B

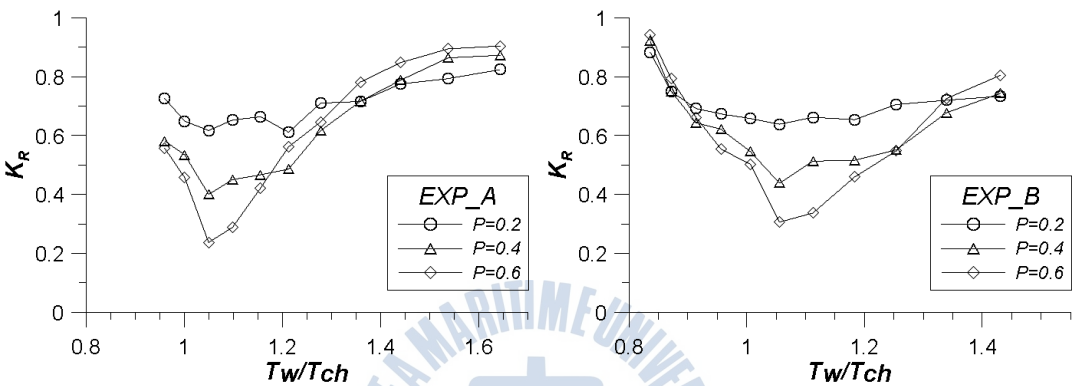

Fig. 5.8 Reflection coefficients K_R of the hydraulic experiment (single channel case: A and B)

(a) single $(AB(1))$ (b) double $(AB(2))$

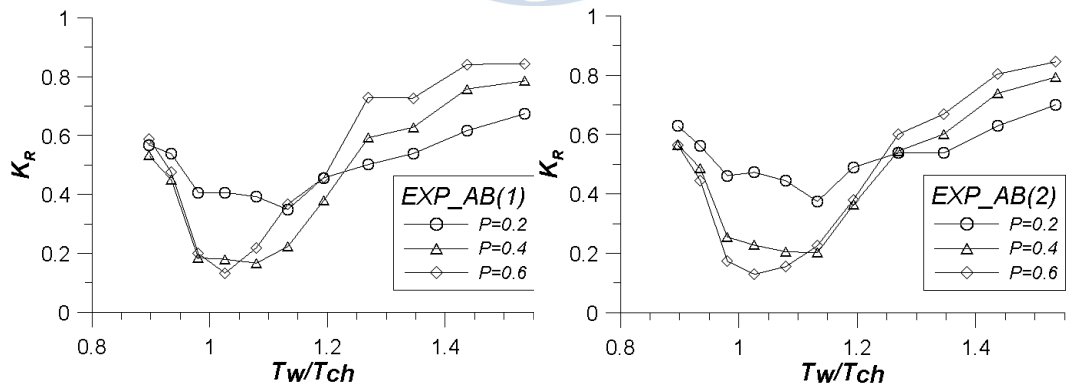

Fig. 5.9 Reflection coefficients K_R of the hydraulic experiment (comparing single($AB(1)$) and double($AB(2)$) channel case)

(a) single ($ABC(1)$) (b) triple ($ABC(3)$)

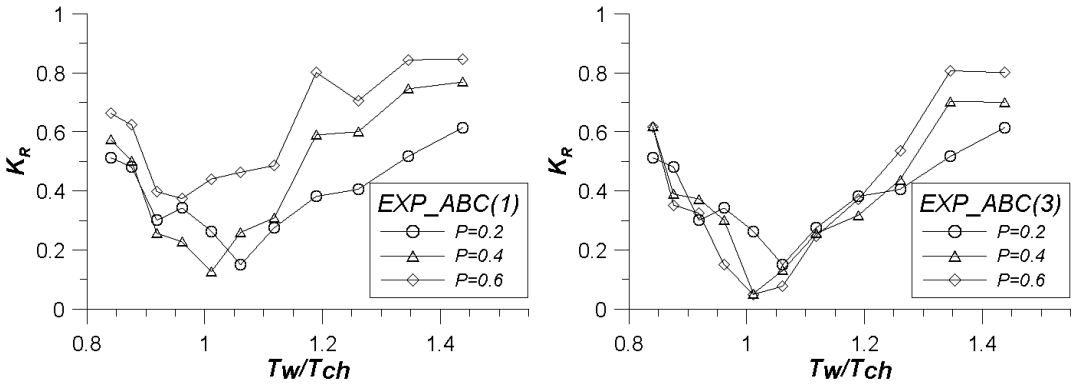

Fig. 5.10 Reflection coefficients K_R of the hydraulic experiment (comparing single($ABC(1)$) and triple($ABC(3)$) channel case)

5.4.2 Comparison of Numerical and Experiment Results

The reflection coefficients are compared with numerical results and hydraulic experiment results for validation of numerical analysis. The each cases are classified by shape of the channel and porosity of the slit plate in the Table 5.1. These are shown in the Fig. 5.11–5.16. In these figures, the solid line is the result of numerical analysis and circle symbols are results of the experiment.

In the entire cases, reflection coefficients of the numerical results and experimental results are properly matched. Exceptionally at the $P=0.6$ and case of $AB(1)$ and $ABC(1)$, the experiment reflection coefficients are more reduced than the numerical results. It means that the optimal porosity region of the numerical analysis are more expanded especially wide channel cases. Also reduced band of reflection coefficients of the experiment are more expanded than the numerical results in wave periods. In this analysis, energy dissipation at the slit plate was only considered. Actually energy dissipation of section contraction also exist at the channel entrance between near fluid field and embedded channel.

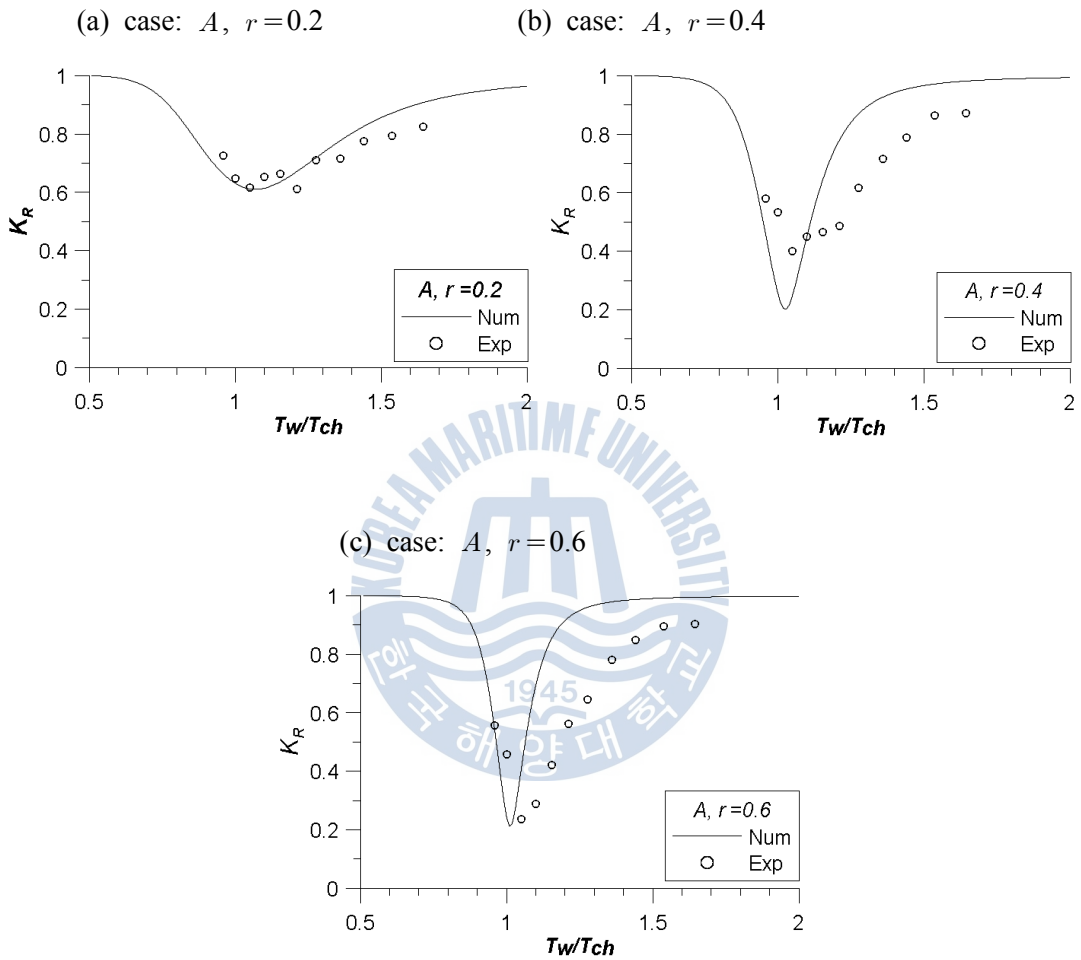

Fig. 5.11 Reflection coefficients K_R of the numerical analysis and hydraulic experiment (case: A, $r=0.2,\ 0.4,\ 0.6$)

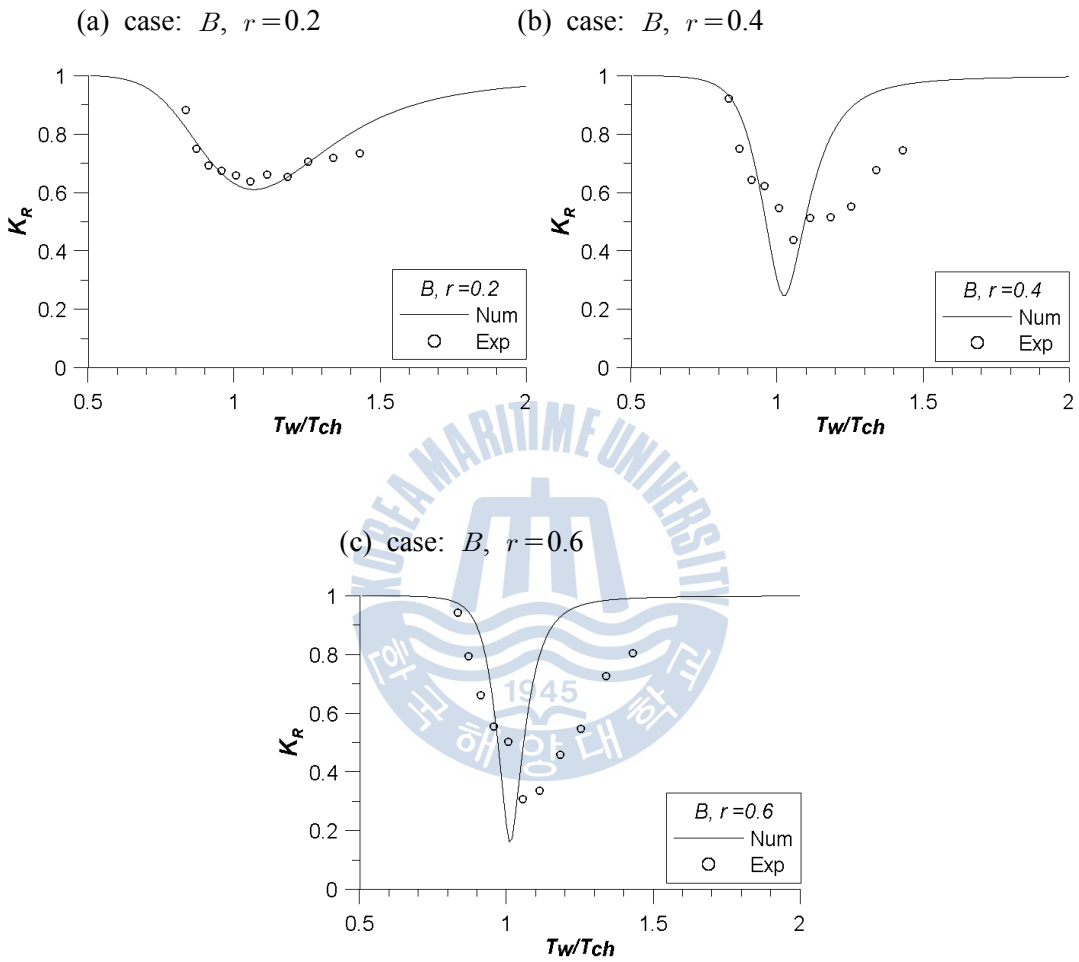

Fig. 5.12 Reflection coefficients K_R of the numerical analysis and hydraulic experiment (case: B, $r=0.2,\ 0.4,\ 0.6$)

(a) case: $AB(1),\ r=0.2$

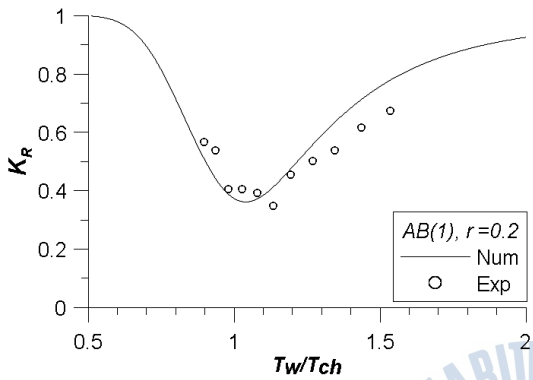

(b) case: $AB(1),\ r=0.4$

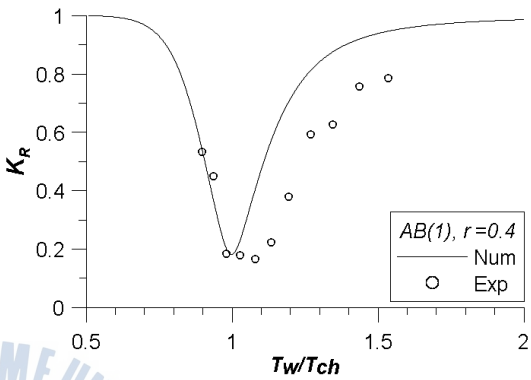

(c) case: $AB(1),\ r=0.6$

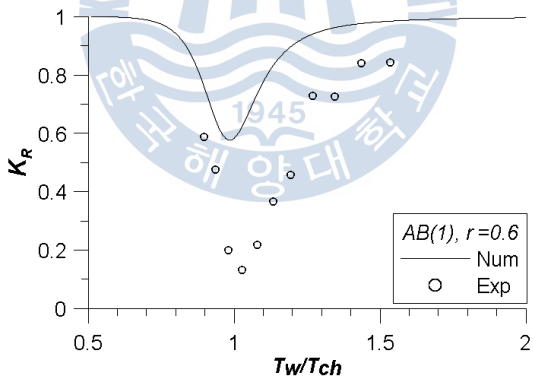

Fig. 5.13 Reflection coefficients K_R of the numerical analysis and hydraulic experiment (case: $AB(1),\ P=0.2,\ 0.4,\ 0.6$)

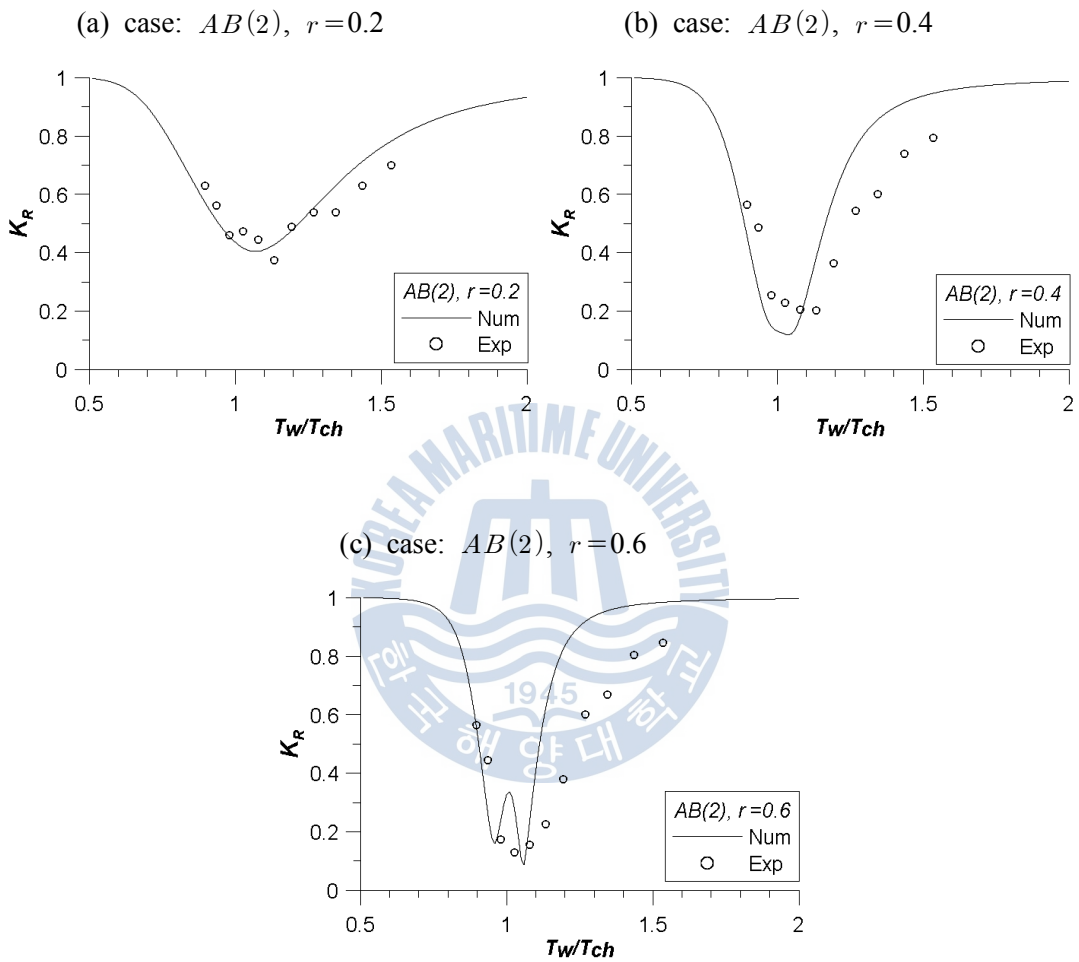

Fig. 5.14 Reflection coefficients K_R of the numerical analysis and hydraulic experiment (case: $AB(2),\ r=0.2,\ 0.4,\ 0.6$)

(a) case: $ABC(1),\ r=0.2$ (b) case: $ABC(1),\ r=0.4$

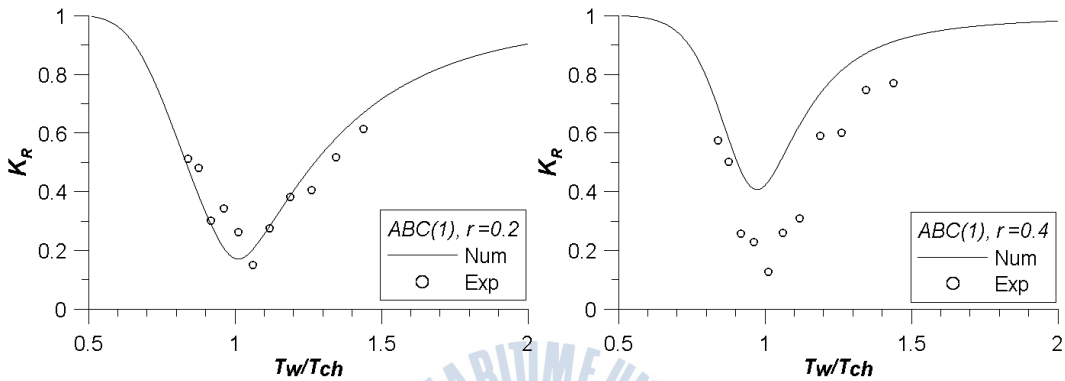

(c) case: $ABC(1),\ r=0.6$

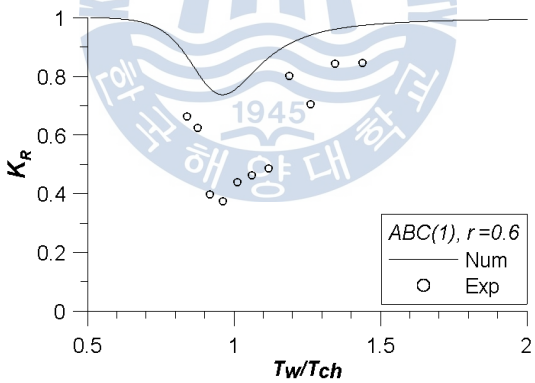

Fig. 5.15 Reflection coefficients K_R of the numerical analysis and hydraulic experiment (case: $ABC(1),\ r=0.2,\ 0.4,\ 0.6$)

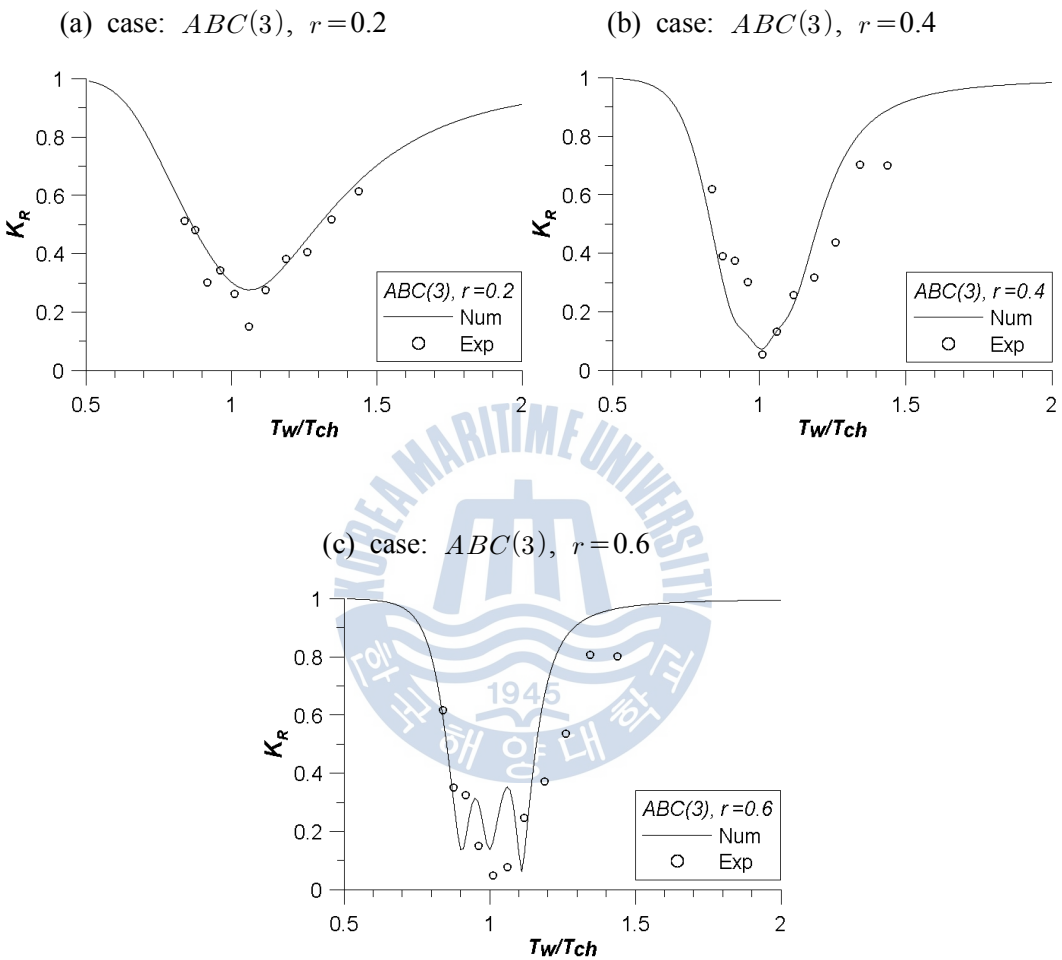

Fig. 5.16 Reflection coefficients K_R of the numerical analysis and hydraulic experiment (case: $ABC(3),\ r=0.2,\ 0.4,\ 0.6$)

CHAPTER 6

CONCLUSIONS

6.1 Conclusions

In the past, various research of reflect waves on perforated-wall caisson breakwater has been proposed and constructed at the coastal area. The water chamber width of this conventional breakwater was critically related with wave node location and wavelength B/L=0.2~0.25 for proper wave energy dissipation. To control the long waves, the chamber width should be horizontally widened in proportion to the wavelength.

The objective of this research was to propose the new concept slit caisson breakwater using embedded channels for reducing the reflected waves. The water column in the embedded channel section has eigenvalue related with mass and restoring forces from shape of water column. The natural period of water column in the channel is critically related with channel length. The amplified flow oscillates between the slit plate in horizontal direction. Therefore the energy dissipation due to flow separation at slit plate is maximized in the resonant condition. The resonant mode of fluid in the channel can be controled by design of channels. Also the design of channel to control the long waves is more resonable than the conventional perforated-wall breakwater.

To evaluate the reflection characteristics, the fluid domain was discretized using Galerkin's finite element method based on linear potential theory. In present study, the used finite element model can consider interaction between waves and slit type structures. The non-linear energy dissipation phenomenon of flow separation at slit

plate is linearized using Lorentz's transformation and averaging power over depth, in which slit plate is consisted by array of rectangular cylinders.

The wave reflection characteristics of slit caisson breakwater with the embedded resonant channel was investigated by numerical analysis and hydraulic model test. The reflection coefficients were influenced by several variables related with the embedded channel and slit plate. These variables are incident wave period T_w, depth of the channel inlet D, width of the channel B, porosity of slit plate r and the number of the embedded channels. Each of variables were influenced on reflection coefficient and analysis of them are follows as:

1) Incident wave period T_w

When the resonant mode of water column in the embedded channel is properly formed, the incident wave energy dissipation is maximized. The resonant period was shown at near matching condition of incident wave period and natural period of the embedded channel $T_w/T_{ch} \simeq 1$. It was effected by width of the embedded channel and porosity of the slit plate. At the condition of low porosity and narrow width of the channel, the resonant periods are moved to longer period especially. It is guessed that the decreased flow into the channel effects to mass of water column in the channel.

2) Depth of the channel inlet D

One of the advantages of using the embedded channel is the protection of slit region from the impact wave loads. For this reason, influence of the channel inlet location on reflection characteristics was analyzed at various water depth. As a result, the effect of the channel inlet depth was small in reflection characteristics. It is estimated that the installed area of the caisson breakwater was finite water

region from the relation of water depth with wave length. At the finite water region, the wave particle motion is flat orbital and it is similar in all water depth. Therefore, the flow entering into the channel by the wave particle motion is hardly affected by the depth of the channel inlet.

3) Porosity of slit plate r

The porosity of slit plate effected to resonant mode of water column in the embedded channel and energy dissipation. The low porosity had affected to reduce the incoming flow into the embedded channel. For this reason, the resonant mode of water column in the embedded channel is difficult to form. At the resonant mode in the channel, the amplified flow passes through the slits and the flow lose the energy by flow separation with empirical contraction of slits. Especially, the low porosity of slit plate affected to the large energy dissipation. From these two perspectives that resonant mode and energy dissipation, the porosity is to be determined in an appropriate evaluation.

4) Width of the embedded channel B

The width of the embedded channel was affected to matching porosity and band width of incident wave periods for proper wave energy dissipation. When the channel width was narrow, the proper energy dissipation was occurred at large porosity and narrow band of incident wave periods. In contrast, the wide width of the channel shows that the proper energy dissipation was occurred at low porosity and wide band of incident wave periods. The channel width and the band width of incident wave periods showed a proportional relationship. On the other hand, the channel width and porosity had a inverse relationship. The results of hydraulic experiment show that the reducing condition (r and B/L_C) of reflection coefficient was more expanded than the results of numerical analysis, especially longer wave

periods than natural period of the channel.

5) Number of channels

The design conditions representing the optimal effect was based on the width of the channel B and porosity of slit plate r. The design parameters according to the target reflection coefficients were proposed as guideline for design of the embedded single channel. In the whole region of multi-channel cases, the upper limit of optimal porosities were satisfied all porosity region. Also the multi-embedded channels separates the natural periods to shorter (upper channel) and longer periods (lower channel) under the reflection coefficient $K_R < 0.2$. From this reason, the incident wave period band of the multi-channel showing the considerably reduced reflection were more expanded than the single channel.

6.2 Future Studies

In this study, the regular waves based on linear potential theory was adopted to interaction problem of wave and structure and the numerical analysis was validated by comparing with hydraulic model test results. In order to describe the sea state, it is necessary to applying the irregular waves and various wave direction. Furthermore, the non-linear wave theory may be required.

The embedded channel shape was considered to constant width from inlet to way out of the channel. The water column's eigenvalue in the channel is related with restoring force of surface at way out and mass of water column. These are critically related with channel shape. The various channel shape would be considered to improve the reducing reflection performance, such as partially extension section or sloping section of the channel.

REFERENCES

Dalymple, R. A., Losada, M. A. and Martin, P. A. (1991). "Reflection and Transmission from porous structures under oblique wave attack." *J. Fluid Mech*, 224, 625-644.

Fugazza, M. and Natale, L. (1992). "Hydraulic design of perforated breakwaters." *J. of Waterway Port Coastal Eng.*, 118, 1-14.

Fujita, T., Matsushita, Y. and Kakuno, S. (2003). "Wave reflection from a slit-type breakwater/seawall having L-shaped Bulkheads inside." *Proc. of 13th Int Offshore and Polar Eng. Conf.*, 664-670.

Goda, Y. (1985). "Random seas and design of maritime structures." Univ. of Tokyo Press.

Goda, Y. and Suzuki, Y. (1976). "Estimation of incident and reflected waves in random wave experiments." *Proc. 15th Coastal Engineering Conference*, 828-845.

Hunt, John N. (1979). "Direct Solution of Wave Dispersion Equation." *J. Waterway, Port, Coastal and Ocean Division.*, ASCE, 105, 5, 457-459.

Kakuno, S. and Oda, K. (1986). "Boundary value analysis on the interaction of cylinder arrays of arbitrary cross-section with train of uniform waves." *J.*

Japanese Soc. Civil Eng., Tokyo, Japan, 369, 213-222 (in Japanese).

Kakuno, S., Oda, K. and Liu, P. L. -F. (1992). "Scattering of water waves by vertical cylinders with a backwall." *Proc. 23rd Coastal Eng. Conf.*, ASCE, Vol 2, 1258-1271.

Kakuno, S. and Liu, P. L. -F. (1993). "Scattering of water waves by vertical cylinders." *J. Waterway, Port, Coastal and Ocean Eng.*, ASCE, 1993(3), 302-322.

Kakuno, S,. Yamono, K.. and Kurata, K. (1995). "An approximated solution for scattering of oblique waves by an array of piles of an arbitrary cross section." *Proc. 5th Int. Offshore and Polar Eng. Conf.,* 3, 162-167.

Kim, B. H. (1998). "Interactions of waves, seabed and structure." Doctorate thesis, Seoul National University.

Kim, B. H., Lee, K. S. and Park, W. S. (1997). "Wave forces on equally spaced vertical piles considering flow separation effects." *7th Int. Conference on Computing in Civil and Building Eng.*, 3, 1649-1654.

Kim, J. S., Seo, J. H., Park, W. S. and Lee J. W. (2014a). "Wave reflections from perforated breakwaters having resonant channels." *Proc. 24th Int. Offshore and Polar Eng. Conf.,* 3, 890-896.

Kim, J. S., Seo, J. H., Lee, J. W. and Park, W. S. (2014b). "Numerical analysis of reflection characteristics of perforated breakwater with a resonant channel." *J.*

Navig. Port Res., 38(5), 503-509 (in Korean).

Kondo, H. (1979). "Analysis of breakwaters having two porous wall." *Proc. Coastal Structure '79*, ASCE, 2, 962-977.

KORDI (1997). "Evaluation and improvement of the performance of wave control structures." 29-40 (in Korean).

Linton, C. M., and Evans, D. V. (1990). "The interaction of waves with array of vertical circular cylinders." *J. Fluid Mech.*, 215, 549-570.

Mansard, E.P.D. and Funk, E.R. (1980). "The measurement of incident and reflected spectra using a least square method." *Proc. 17th Coastal Engineering Conference*, 191-206.

Martin P. A. and Dalryple, R. A. (1988). "Scattering of long waves by cylinders obstacles and gratings using matched asymtotic expansions." *J. Fluid Mech.,* 188, 465-490.

Massel, S. R. (1993). "Extended refraction-diffraction equation for surface waves." *Coastal Eng.*, 19, 97-126.

Park, W. S., Chun, I. S. and Lee, D. S. (1993). "Hydraulic experiments for the reflection characteristics of perforated breakwaters." *J. Korean Soc. of Coastal and Ocean Eng.,* 5(3), 198-203.

Park, W. S., Lee, D. S., Oh, Y. M. and Jeong, W. M. (1991). "Infinite elements

for analysis of diffraction and radiation problems in the vertical plane." *J. Korean Soc. of Coastal and Ocean Eng.*, 3(4), 235-243 (in Korean).

Park, W. S., Oh, Y. M. and Chun, I. S. (1992). “Separation technique of incident and reflected waves using least squares method.” *J. Korean Soc. of Coastal and Ocean Eng.*, 4(3), 139-145 (in Korean).

Park, W. S. and Takahashi, S. (1996). "FEM simulation of wave-soil-structure interaction problems." *3rd Asian-Pacific Conf. on Computational Mech.*, 845-850.

Suh, K. D. (1996). "Wave reflection from partially perforated caisson breakwater." *J. Korean Soc. of Coastal and Ocean Eng.*, 8(3), 221-230.

Suh, K. D., Park, J. K. and Park, W. S. (2006). "Wave reflection from partially-perforated-wall caisson breakwaters." *J. of Ocean Eng.*, 33, 264-280.

Suh, K. D. and Park, W. S. (1995). "Wave reflection from perforated-wall caisson breakwaters." *Coastal Eng.*, 26, 177-193.

Taylor, P. J. (1973). “The Coefficient for flow about an arbitrary body immersed in a channel.” *J. of Ship Res.*, 17, 97-105.

APPENDICES

A.1 Derivation of $M_i(\xi)$ and $M_o(\xi)$

A.2 Determination of A_{ij} and B_{ij}

APPENDICES

A.1 Derivation of $M_i(\xi)$ and $M_o(\xi)$

The scattered wave potential, ϕ_j, can be represented by a series of eigenfunctions:

$$\phi_j = a_o \cosh[k(z+h)]e^{ikr} + \sum_{m=1}^{\infty} b_m \cos[k_m(z+h)]e^{-k_m r} \tag{A.1.1}$$

in which k and k_m = the positive real roots of the equivalent dispersion relations such as

$$k \tanh kh = \frac{\omega^2}{g} \tag{A.1.2}$$

$$k_m \tan k_m h = -\frac{\omega^2}{g} \tag{A.1.3}$$

The behavior of the scattered wave potential in the horizontal direction may be represented approximately as two terms with the progressive wave and the first evanescent wave components such as

$$\phi_j \approx a_1 e^{ikr} + b_1 e^{-k_1 r}$$

$$= \begin{bmatrix} \overline{f_o}(r) \\ \overline{f_1}(r) \end{bmatrix}^T \begin{bmatrix} a_1 \\ b_1 \end{bmatrix} \tag{A.1.4}$$

in which a_1 and b_1 are the known coefficients.

To determine the shape functions in the horizontal direction, consider the nodal potentials, ϕ_a and ϕ_b located at r_a and r_b from the origin, respectively.

Evaluating the nodal potentials, ϕ_a and ϕ_b, from Eq. (A.2.4)

$$\begin{bmatrix} \phi_a \\ \phi_b \end{bmatrix} = \begin{bmatrix} \overline{f_o}(r) & \overline{f_1}(r) \\ \overline{f_o}(r) & \overline{f_1}(r) \end{bmatrix} \begin{bmatrix} a_1 \\ b_1 \end{bmatrix} \tag{A.1.5}$$

from which the inverse is

$$\begin{bmatrix} a_1 \\ b_1 \end{bmatrix} = F \begin{bmatrix} \phi_a \\ \phi_b \end{bmatrix} \tag{A.1.6}$$

in which

$$F = \begin{bmatrix} e^{ikr_i} & e^{-k_1 r_i} \\ e^{ik_o r_o} & e^{-k_1 r_o} \end{bmatrix}^{-1} \tag{3.16}$$

and by substituting Eq. (A.2.6) into Eq. (A.2.4),

$$\phi_j = \begin{bmatrix} M_i(\xi) \\ M_o(\xi) \end{bmatrix} \begin{bmatrix} \phi_a \\ \phi_b \end{bmatrix} \tag{A.1.7}$$

in which

$$\begin{bmatrix} M_i(\xi) \\ M_o(\xi) \end{bmatrix} = F^T \begin{bmatrix} \overline{f_o}(\xi+r_a) \\ \overline{f_o}(\xi+r_a) \end{bmatrix} \tag{A.1.8}$$

with $\xi = r - r_a$

The system matrix of an infinite element can not be constructed uniquely, since the integrated value in the ξ-direction does not exist. Thus, the above shape functions are slightly modified with introducing the artificial decaying parameter, $\epsilon_d \ (0 < \epsilon_d \ll k)$ as

$$f_o(\xi) = \overline{f_o}(\xi+r_a) e^{-\epsilon_d \xi} \tag{3.14}$$

$$f_1(\xi) = \overline{f_1}(\xi+r_a) \tag{3.15}$$

Accordingly, $M_i(\xi)$ and $M_o(\xi)$ can be rewritten as

$$\begin{bmatrix} M_i(\xi) \\ M_o(\xi) \end{bmatrix} = F^T \begin{bmatrix} \overline{f_o}(\xi) \\ \overline{f_1}(\xi) \end{bmatrix} \tag{3.13}$$

A.2 Determination of A_{ij} and B_{ij}

A_{ij} and B_{ij} are defined as the matrix form

$$A = \begin{bmatrix} A_{11} & A_{12} \\ A_{21} & A_{22} \end{bmatrix} = F^T \begin{bmatrix} \overline{A}_{11} & \overline{A}_{12} \\ \overline{A}_{21} & \overline{A}_{22} \end{bmatrix} F^T \tag{A.2.1}$$

$$B = \begin{bmatrix} B_{11} & B_{12} \\ B_{21} & B_{22} \end{bmatrix} = F^T \begin{bmatrix} \overline{B}_{11} & \overline{B}_{12} \\ \overline{B}_{21} & \overline{B}_{22} \end{bmatrix} F^T \tag{A.2.2}$$

in which the matrix F is appeared in Eq. (3.16), $\overline{A}_{ij}$ and $\overline{B}_{ij}$ are the complex valued coefficients associated with the integration in ξ-direction as follows.

$$\overline{A}_{11} = \int_0^\infty (ik-\epsilon_d)^2 e^{2ik(\xi+r_i)-2\epsilon_d\xi} d\xi \tag{A.2.3a}$$

$$\overline{A}_{12} = \int_0^\infty (ik-\epsilon_d)(-k)\, e^{(ik-k_1)(\xi+r_i)-\epsilon_d\xi} d\xi \tag{A.2.3b}$$

$$\overline{A}_{22} = \int_0^\infty (-k)^2\, e^{-2k_1(\xi+r_i)} d\xi \tag{A.2.3c}$$

$$\overline{B}_{11} = \int_0^\infty e^{2ik(\xi+r_i)-2\epsilon_d\xi} d\xi \tag{A.2.3d}$$

$$\overline{B}_{12} = \int_0^\infty e^{(ik-k_1)(\xi+r_i)-\epsilon_d\xi} d\xi \tag{A.2.3e}$$

$$\overline{B}_{22} = \int_0^\infty e^{-2k_1(\xi+r_i)-\epsilon_d\xi} d\xi \tag{A.2.3f}$$

After integrating the above equations with respect to ξ from 0 to ∞, and taking $\epsilon_d = 0$, then $\overline{A}_{ij}$ and $\overline{B}_{ij}$ can be obtained as a function of k, k_1 and r_i, which are given by

$$\overline{A}_{11} = -\frac{k}{2} e^{2ikr_i} \tag{A.2.4a}$$

$$\overline{A}_{12} = i\frac{kk_1}{ik - k_1} e^{(ik-k_1)r_i} \tag{A.2.4b}$$

$$\overline{A}_{22} = \frac{k_1}{2} e^{-2k_1 r_i} \tag{A.2.4c}$$

$$\overline{B}_{11} = \frac{i}{2k} e^{2ikr_i} \tag{A.2.4d}$$

$$\overline{B}_{12} = -\frac{1}{ik - k_1} e^{(ik-k_1)r_i} \tag{A.2.4e}$$

$$\overline{B}_{22} = \frac{1}{2k_1} e^{-2k_1 r_i} \tag{A.2.4f}$$